

# Radical chemistry in the Pearl River Delta: observations and modeling of OH and HO<sub>2</sub> radicals in Shenzhen 2018

Xinping Yang<sup>1,2</sup>, Keding Lu<sup>1,2,\*</sup>, Xuefei Ma<sup>1,2</sup>, Yue Gao<sup>1,2</sup>, Zhaofeng Tan<sup>3</sup>, Haichao Wang<sup>4</sup>, Xiaorui Chen<sup>1,2</sup>, Xin Li<sup>1,2</sup>, Xiaofeng Huang<sup>5</sup>, Lingyan He<sup>5</sup>, Mengxue Tang<sup>5</sup>, Bo Zhu<sup>5</sup>, Shiyi Chen<sup>1,2</sup>, Huabin Dong<sup>1,2</sup>, Limin Zeng<sup>1,2</sup>, Yuanhang Zhang<sup>1,2,\*</sup>

<sup>1</sup>State Key Joint Laboratory of Environmental Simulation and Pollution Control, College of Environmental Sciences and Engineering, Peking University, Beijing, China

<sup>2</sup>State Environmental Protection Key Laboratory of Atmospheric Ozone Pollution Control, Peking University, Beijing, China

<sup>3</sup>Institute of Energy and Climate Research, IEK-8: Troposphere, Forschungszentrum Juelich GmbH, Juelich, Germany

<sup>4</sup>School of Atmospheric Sciences, Sun Yat-Sen University, Zhuhai, China

<sup>5</sup>Laboratory of Atmospheric Observation Supersite, School of Environment and Energy, Peking University Shenzhen Graduate School, Shenzhen, China

Correspondence to: Keding Lu ([k.lu@pku.edu.cn](mailto:k.lu@pku.edu.cn)), Yuanhang Zhang ([yhzhang@pku.edu.cn](mailto:yhzhang@pku.edu.cn))

**Abstract.** The ambient radical concentrations were measured continuously by laser-induced fluorescence during the STORM (STudy of the Ozone foRmation Mechanism) campaign at the Shenzhen site, located in the Pearl River Delta in China, in the autumn of 2018. The diurnal maxima were  $4.5 \times 10^6 \text{ cm}^{-3}$  for OH and  $4.54.2 \times 10^8 \text{ cm}^{-3}$  for HO<sub>2</sub> (including an estimated interference of 23%-28% from RO<sub>2</sub> radicals during the daytime), respectively. The state-of-the-art chemical mechanism underestimated the observed OH concentration, similar to the other warm-season campaigns in China. The OH underestimation was attributable to the missing OH sources, which can be explained by the X mechanism. Good agreement between the observed and modeled OH concentrations was achieved when an additional numerical X equivalent to 0.1 ppb NO concentrations was added into the base model. The isomerization mechanism of RO<sub>2</sub> derived from isoprene contributed approximately 7% to the missing OH sources-production rate and the oxidation of isoprene oxidation products (MACR and MVK) had no significant impact on the missing OH sources, demonstrating further exploration of unknown OH sources is necessary. A significant HO<sub>2</sub> heterogeneous uptake was found in this study, with an effective uptake coefficient of 0.3. The ROx primary production rate was dominated by photolysis reactions, dominated the ROx primary production rate, in which the HONO, O<sub>3</sub>, HCHO, and carbonyls photolysis accounted for 29%, 16%, 16%, and 11% during the daytime, respectively. The ROx termination rate was dominated by the reaction of OH + NO<sub>2</sub> in the morning, and thereafter the radical self-combination gradually became the major sink of ROx in the afternoon. As the sum of the respective oxidation rates of the pollutants via reactions with oxidants, the atmospheric oxidation capacity was evaluated, with a peak of 11.8 ppb h<sup>-1</sup> around noontime. The ratio of  $P(\text{O}_3)_{\text{net}}$  to  $\text{AOC}_{\text{VOCs}}$ , which indicates the yield of net O<sub>3</sub>-ozone production from VOCs oxidation, trended to increase and then decrease as the NO concentration increased. The median ratios ranged within 1.0-4.5, with Additionally, the maximum of the ratios existed when the NO concentration was approximately 1 ppb, with a median of about 2.

带格式的: 下标

34 ~~indicating that the yield of ozone production from VOCs oxidation was about 2 in this campaign. The nonlinear relationship~~  
35 ~~between the yield of net ozone production from VOCs oxidation and NO concentrations demonstrated that optimizing the NOx~~  
36 ~~and VOCs control strategies is critical to control the ozone pollution effectively in the future.~~  
37 \_\_\_\_\_

带格式的: 字体颜色: 自动设置

## 38 1 Introduction

39 Severe ambient ozone (O<sub>3</sub>) pollution is one of China's most significant environmental challenges, especially in urban areas  
40 (Shu et al., 2020; Li et al., 2019; Wang et al., 2020; Ma et al., 2019b; Wang et al., 2017a). Despite the reduction in emissions of  
41 O<sub>3</sub> precursors, O<sub>3</sub> concentration is increasing, especially in urban cities. The O<sub>3</sub> average trends for the focus megacity clusters  
42 are 3.1 ppb a<sup>-1</sup>, 2.3 ppb a<sup>-1</sup>, 0.56 ppb a<sup>-1</sup>, and 1.6 ppb a<sup>-1</sup> for North China Plain (NCP), Yangtze River Delta (YRD), Pearl River  
43 Delta (PRD), and Szechwan Basin (SCB), respectively (Li et al., 2019). The nonlinearity between O<sub>3</sub> and precursors illustrates  
44 that it is necessary to explore the cause of O<sub>3</sub> production. The tropospheric O<sub>3</sub> is only generated in the photolysis of nitrogen  
45 dioxide (NO<sub>2</sub>), which is produced as the by-product within the radical cycling. Thus, the investigation of radical chemistry is  
46 critical to controlling secondary pollution.

47 Hydroxyl radicals (OH), the dominant oxidant, control the atmospheric oxidation capacity (AOC) in the troposphere. The  
48 OH radicals convert primary pollutants to secondary pollutants and are simultaneously transformed into peroxy radicals (HO<sub>2</sub>  
49 and RO<sub>2</sub>). Within the interconvert of ROx (= OH, HO<sub>2</sub>, and RO<sub>2</sub>), secondary pollutants are generated, and thus the further  
50 exploration of radical chemistry is significant. The radical closure experiment, an effective indicator for testing our  
51 understanding of radical chemistry, has been conducted since the central role of OH radicals was recognized in the 1970s (Levy,  
52 1971; Hofzumahaus et al., 2009). The underestimation of OH radicals in environments characterized by low nitrogen oxides  
53 (NO) and high volatile organic compounds (VOCs) has been identified (Lu et al., 2013; Lu et al., 2012; Tan et al., 2017; Tan et  
54 al., 2019; Yang et al., 2021; Hofzumahaus et al., 2009; Lelieveld et al., 2008; Whalley et al., 2011). New radical mechanisms  
55 involving unclassical OH regeneration have been proposed, mainly including Leuven Isoprene Mechanism (LIM) and X  
56 mechanism (Peeters and Muller, 2010; Peeters et al., 2014; Peeters et al., 2009; Hofzumahaus et al., 2009). The LIM which has  
57 been ineoperated-integrated into the current radical mechanism and is still insufficient to explain the OH missing sources.  
58 The X mechanism was identified several times, but the amount of the numerical species, X, varied in different environments,  
59 and the nature of X is still unknown (Hofzumahaus et al., 2009; Lu et al., 2013; Lu et al., 2012; Tan et al., 2017; Tan et al.,  
60 2019; Yang et al., 2021; Ma et al., 2022a). Therefore, further exploration of radical regeneration sources is necessary.

61 Due to the strong photochemistry influenced by high temperatures and strong radiation, high O<sub>3</sub> pollution appeared to occur  
62 in YRD and PRD, especially in PRD (Ma et al., 2019b; Wang et al., 2017a). Radicals, the dominant oxidant in the troposphere,  
63 have been measured during warm seasons in NCP (Yufa 2006, Wangdu 2014, and Beijing 2016), YRD (Taizhou 2018), SCB  
64 (Chengdu 2019), and PRD (Backgarden 2006, and Heshan 2014) in China (Lu et al., 2013; Lu et al., 2012; Tan et al., 2017; Tan  
65 et al., 2019; Yang et al., 2021; Tan et al., 2021; Ma et al., 2022a). The radical observations in PRD, where the cities are suffering  
66 from severe O<sub>3</sub> pollution, have not been conducted since 2014, and thus the oxidation capacity here has not been clear in recent  
67 years. Therefore, we carried out a continuous comprehensive field campaign (STudy of the Ozone foRmation Mechanism -  
68 STORM) involving radical observations in Shenzhen, one of the megacities in PRD, in autumn 2018. Overall, the following

will be reported in this study.

(1) The observed radical concentrations, and the comparison between the radical observations and simulations.

(2) The exploration of the unclassical OH regeneration sources based on the experimental budget.

(3) The sources and sinks of ROx radicals.

(4) The evaluation of the atmospheric oxidation capacity.

## 2 Methodology

### 2.1 Measurement site and instrumentation

The STORM campaign was conducted from September to October 2018 in Peking University Shenzhen Graduate School (22.60 deg N, 113.97 deg E), in the west of Shenzhen, Guangdong province. As shown in Fig. 1, this site, which belongs to the urban site, is located in the university town, and is surrounded by residential and commercial areas. The northwest of the site is close to the Shenzhen Wildlife Park, and the northeast is close to the Xili Golf Club (Yu et al., 2020). The Tanglang Mountain Park with active biogenic emissions is located about 1 km southeast of the site. Overall, this site has no significant local pollution sources nearby, but can represent the urban pollution characteristics (Huang et al., 2012a; Huang et al., 2012b; Gao et al., 2018).



Figure 1: Geographical location and surrounding environmental conditions of the measurement site in STORM campaign (The maps are from <https://map.baidu.com>).

Most instruments were set up on the top of a four-story academic building (about 20 m). Besides HOx radicals measured by the Peking University-Laser-Induced Fluorescence system (PKU-LIF) (see the details in Sect. 2.2), a comprehensive set of trace gases was conducted to support the exploration of the radical chemistry, including meteorological parameters (temperature, pressure, relative humidity, *etc.*), photolysis frequency, OH reactivity ( $k_{OH}$ ) and the trace gases (NO, NO<sub>2</sub>, O<sub>3</sub>, VOCs, *etc.*).  $k_{OH}$  was measured by the Laser flash photolysis-Laser induced fluorescence (LP-LIF) system. Most of the inorganic trace gases (O<sub>3</sub>, CO, NO, NO<sub>2</sub>, and SO<sub>2</sub>) were simultaneously measured by two sets of instruments, and good

带格式的: 字体: 倾斜

92 agreement was achieved within the uncertainty. VOCs [species](#) ([aldehydes](#)[alkanes](#), alkenes, aromatics, isoprene, and  
93 oxygenated VOCs (OVOCs)) were measured using a gas chromatograph following a mass spectrometer (GC-MS). In addition,  
94 HONO and HCHO were measured as well. Table S1 in the Supplementary Information [describes](#)[presents](#) the experimental  
95 details of the meteorological and chemical parameters during this campaign.

## 96 2.2 The OH and HO<sub>2</sub> measurements

97 The OH and HO<sub>2</sub> radicals were measured by [Peking University laser induced fluorescence system](#) (PKU-LIF) based on the  
98 fluorescence assay by gas expansion (FAGE) technique. The principle has been reported in previous studies, only a brief  
99 description of the instrument is presented here. Further detailed information on the instrument can be found in previous studies  
100 (Heard and Pilling, 2003; Fuchs et al., 2008; Holland et al., 1995; Hofzumahaus et al., 1996; Fuchs et al., 2011).

101 In principle, OH resonance fluorescence is released in the OH excitation by a 308 nm pulsed laser, and then OH radicals are  
102 detected directly. HO<sub>2</sub> radicals are converted into OH via NO, and then they are detected. The system contains a laser module  
103 and a detection module. Ambient air was drawn into two independent, parallel, low-pressure (3.5 mBar) cells through two  
104 parallel nozzles with 0.4 mm diameter pinhole. The OH radicals are excited into resonance fluorescence in the OH detection  
105 cell and detected by micro-channel plate detectors (MCP). In the HO<sub>2</sub> detection cell, NO is injected and converts HO<sub>2</sub> to OH  
106 radicals, [which](#)[and](#) then [OH radicals](#) are excited by the laser and release resonance fluorescence. Besides, an OH reference  
107 cell in which a large OH concentration is generated by pyrolysis of water vapor on a hot filament is applied to automatically  
108 correct the laser wavelength.

109 Owing to the failure of the reference cell in this [study](#)[campaign](#), the NO mixing ratios injected into the HO<sub>2</sub> [detection](#) cell  
110 were set to be higher than that in other campaigns in China because the HO<sub>2</sub> cell needed to be used as a reference cell to correct  
111 laser wavelength. In this campaign, NO mixing ratios were switched between 25 ppm (low NO mode) and 50 ppm (high NO  
112 mode). We calculated the HO<sub>2</sub>-to-OH conversion [rates](#)[efficiencies](#) under the two different NO concentrations by calibrating  
113 the PKU-LIF system. HO<sub>2</sub>-to-OH conversion [efficiencies](#)[rates](#) in low NO mode ranged within 80%-95%, while those in high  
114 NO mode [were overreached](#) 100%, demonstrating that [the high NO concentration is sufficiently to achieve complete HO<sub>2</sub> to](#)  
115 [OH conversion and thus](#) the HO<sub>2</sub> measurement was affected by RO<sub>2</sub> radicals. Prior studies have reported the relative detection  
116 sensitivities ( $\alpha_{RO_2}$ ) for the major RO<sub>2</sub> species, mainly from alkenes, isoprene and aromatics, when the HO<sub>2</sub>-to-OH conversion  
117 [efficiencies](#)[rate was over reach](#) 100% (Fuchs et al., 2011; Lu et al., 2012; Lu et al., 2013). [Therefore](#)[Herein](#), only the HO<sub>2</sub>  
118 observations in high NO mode were chosen and they were denoted as [HO<sub>2</sub>\*], which was the sum of the true HO<sub>2</sub> concentration  
119 and a systematic bias from the mixture of RO<sub>2</sub> species  $i$  which were detected with different relative sensitivities  $\alpha_{RO_2}^i$ , as  
120 shown in Eq. (1) (Lu et al., 2012). The true HO<sub>2</sub> concentration was difficult to calculated because the RO<sub>2</sub> concentration  
121 measurements and their speciation were not available. Herein, we simulated the HO<sub>2</sub> and HO<sub>2</sub>\* concentrations by the model,  
122 [and the RO<sub>2</sub> interference yields which was used for correction were the modeled values reported by Lu et al. \(2012\)](#). The

123 interference from RO<sub>2</sub> radicals was estimated to be the difference between the modeled HO<sub>2</sub> and HO<sub>2</sub><sup>\*</sup> concentrations. Overall,  
124 the measurement uncertainties of OH and HO<sub>2</sub><sup>\*</sup> radicals were 11% and 15%, respectively, as shown in Table S1 in the  
125 Supplementary Information.

$$126 [\text{HO}_2^*] = [\text{HO}_2] + \sum(\alpha_{\text{RO}_2}^i \times [\text{RO}_2]_i) \quad (1)$$

127 Additionally, prior studies reported that OH measurement might be affected by the potential interference, when the sampled  
128 air contained ozone, alkenes and BVOCs (Mao et al., 2012; Fuchs et al., 2016; Novelli et al., 2014), indicating the environmental  
129 conditions are important to the production of interference. The pre-injector is usually used to test the potential OH interference,  
130 and has been applied to our PKU-LIF system to quantify the possible interferences for several campaigns, including the  
131 campaigns conducted ~~in at the~~ Wangdu, Heshan, Huairou, Taizhou and Chengdu sites (Tan et al., 2017; Tan et al., 2019; Tan et  
132 al., 2018; Yang et al., 2021). No significant internal interference was found in the prior studies, demonstrating the accuracy of  
133 the PKU-LIF system has been determined for several times. Moreover, to further explore the potential interference in this  
134 campaign, we compared the major environmental conditions, especially O<sub>3</sub>, alkenes and isoprene, between Shenzhen and  
135 Wangdu sites, as shown in the Supplementary Information. The results indicated that ~~the~~ the environmental condition in  
136 Shenzhen was less conducive to generating interference than that in Wangdu, and the details were presented in the  
137 Supplementary Information. Besides the environmental conditions, the prior studies reported that the product of the reaction  
138 of RO<sub>2</sub> with OH, trioxides (ROOOH), might lead to an OH interference signal. The reactions of RO<sub>2</sub> radicals with OH radicals  
139 might be competitive with other sinks for RO<sub>2</sub> radicals (Fittschen, 2019; Fittschen et al., 2019; Berndt et al., 2022). However,  
140 Fittschen et al. (2019) reported that the ROOOH interference is highly dependent on the design and measurement conditions  
141 of different FAGE instruments. Therefore, we integrated the reactions of the ROOOH production and destruction into the base  
142 model herein, with the ROOOH production rate constant of 1.5×10<sup>-10</sup> cm<sup>3</sup> s<sup>-1</sup> and the destruction rate constant of 10<sup>-4</sup> s<sup>-1</sup> (the  
143 details are presented in the Supplementary Information) (Fittschen et al., 2019). Figure. S1 (a) presents the modeled ROOOH  
144 concentrations during this campaign, with ~~the~~ a maximum of about 4.4×10<sup>9</sup> cm<sup>-3</sup>. The correlation of the modeled ROOOH  
145 concentrations and the ratios of OH observations to OH simulations, and the correlation of the modeled ROOOH  
146 concentrations and the difference between OH observations and simulations both demonstrated that no significant relevance  
147 between ROOOH and the underestimation of OH radicals, as shown in Fig. S1 (b-c). Additionally, the ROOOH values modeled  
148 in our another campaign (Taizhou, 2018) were comparable to or even slightly higher than the simulations in this study, and the  
149 chemical modulation tests in Taizhou confirmed the ROOOH is not a significant OH interference in our PKU-LIF system (Ma  
150 et al., 2022b). Nevertheless, as shown in Fig. S1 (b-d), the modeled OH, HO<sub>2</sub>, and HO<sub>2</sub><sup>\*</sup> concentrations were not affected by  
151 the ROOOH production and destruction, indicating that the ROOOH interference in this study was negligible. Overall, the OH  
152 interference during this campaign was negligible according to the analysis of the behavior of PKU-LIF system in previous  
153 campaigns, the comparison of environmental conditions ~~during~~ between this campaign and Wangdu campaign, and the

带格式的: 字体: 10 磅

带格式的: 字体: 10 磅

带格式的: 字体: 10 磅

154 ~~exploration of the impact of ROOOH on the discrepancy of OH observations and simulations~~interference on radical  
155 ~~observations.~~ However, we should acknowledge that the unmeasured interference might have an effect on radical measurement.  
156 ~~More precise chemical modulation tests are needed in the future~~Therefore, it is not expected that the OH measurements in this  
157 ~~campaign were affected by the internal interference.~~ Overall, the measurement uncertainties of OH and HO<sub>2</sub> radicals were  
158 ~~11% and 15%, respectively, as shown in Table S1 in the Supplementary Information.~~

带格式的: 字体: 10 磅

### 160 2.3 Closure experiment

161 As an effective tool to explore the atmospheric radical chemistry, the radical closure experiment can investigate the state-of-  
162 the-art chemical mechanism because of the extremely short lifetime of radicals (Stone et al., 2012; Lu et al., 2019). A zero-  
163 dimensional box model was used to conduct the radical closure experiment, and the overall framework was reported by Lu et  
164 al. (2019). In this work, we conducted the radical closure experiment based on the Regional Atmospheric Chemical Mechanism  
165 updated with the latest isoprene chemistry (RACM2-LIM1), as Tan et al. (2017) described in detail. The model was constrained  
166 ~~byte~~ the measured meteorological, photolysis frequency, and the critical chemical parameters (CO, NO, NO<sub>2</sub>, VOCs, etc.). The  
167 H<sub>2</sub> and CH<sub>4</sub> mixing ratios were set to 550 ppb and 1900 ppb, respectively. The model was operated in time-dependent mode  
168 with a 5-min time resolution, and a 2-d spin-up time was to make the unconstrained species approach the steady state relative  
169 to the constrained species.

170 As Lu et al. (2012) described, there are two types of radical closure experiment. One is the comparison of observed and  
171 modeled radical concentrations, and the other is the comparison of radical production and destruction rates. The most  
172 significant difference between the above is that the latter is conducted with the observed radical concentrations and  $k_{OH}$   
173 constrained. The comparison of radical production and destruction rates, ~~which is~~ also called radical experimental budget, can  
174 test the accuracy of the state-of-the-art chemistry mechanisms based on the equivalent relationship between the radical  
175 production and destruction rates. The production rates of OH, HO<sub>2</sub>, and RO<sub>2</sub> radicals are quantified from all the known sources.  
176 The destruction rates of HO<sub>2</sub> and RO<sub>2</sub> radicals are the sum of the known ~~source~~sinks, ~~while,~~ ~~T~~the OH destruction rate can be  
177 directly calculated as the product of the observed OH concentrations and the observed  $k_{OH}$  (Tan et al., 2019; Yang et al., 2021).  
178 The OH destruction rate is the total sinks of OH radicals because of the direct  $k_{OH}$  observation, and thus the discrepancy  
179 between the OH destruction and production rates denotes the missing OH sources. The detailed reactions and the reaction rate  
180 constants related to OH, HO<sub>2</sub>, and RO<sub>2</sub> radicals can be found in Tan et al. (2019) and Yang et al. (2021).

### 181 2.4 AOC evaluation

182 The life time of the trace gases is controlled not only by the oxidant concentration but also by its second-order rate constant,  
183 so the atmospheric oxidation capacity (AOC) proposed by Geyer et al. (2001) is most suitable to evaluate the relative

184 importance of each oxidant (Elshorbany et al., 2009). AOC is the core driving force of complex air pollution, and determines  
185 the removal rate of trace gases and the production rates of secondary pollutants (Liu et al., 2021). As an effective indicator for  
186 atmospheric oxidation intensity, the evaluation of AOC can provide crucial information on the atmospheric composition of  
187 harmful and climate forcing species (Elshorbany et al., 2009). AOC is defined as the sum of the respective oxidation rates of  
188 the pollutants via reactions with oxidants (Elshorbany et al., 2009;Geyer et al., 2001;Zhu et al., 2020). According to the  
189 definition of AOC, it can be calculated by the Eq. (2).

$$190 \text{ AOC} = \sum_i k_{Y_i}[Y_i][X] \quad (2)$$

191 where  $Y_i$  are the pollutants (CO, CH<sub>4</sub>, and VOCs),  $X$  are the main atmospheric oxidants (OH, O<sub>3</sub>, NO<sub>3</sub>), and  $k_{Y_i}$  is the bi-  
192 molecular rate constant for the reaction of  $Y_i$  with  $X$ . AOC includes all combination of pollutants  $Y$  and oxidants  $X$ . The  
193 higher AOC, the higher removal rate of the most-atmospheric pollutants, and thus the higher production rate of secondary  
194 pollutants (Yang et al., 2020b). Simultaneous measurements of OH and the key trace gases are available in the study. NO<sub>3</sub>  
195 concentration could be simulated by the box model with the observed parameters constrained.

带格式的: 字体: 倾斜

带格式的: 字体: 倾斜

### 196 3. Results

#### 197 3.1 Meteorological and chemical conditions

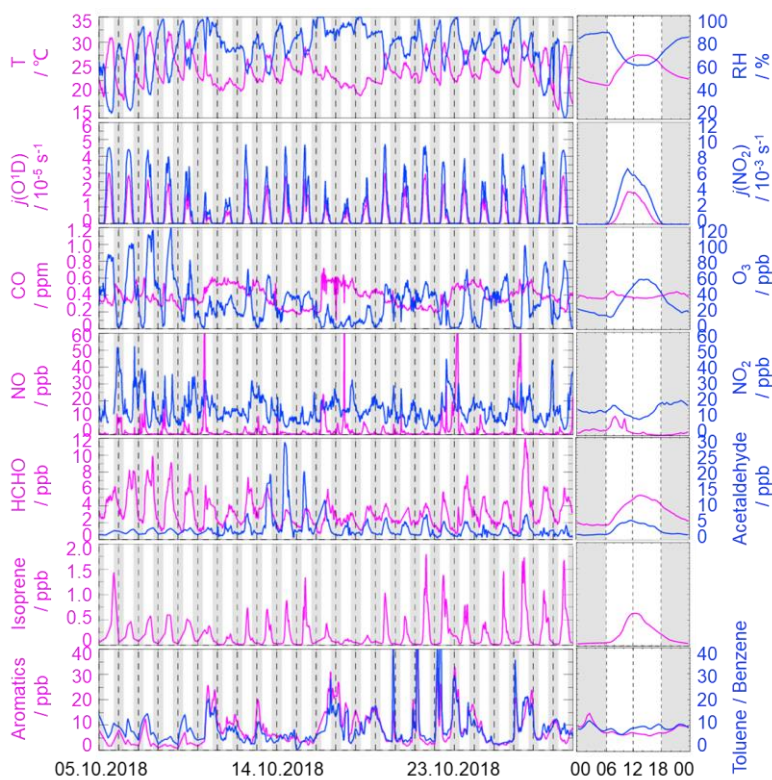
198 Figure 2 gives an overview of the meteorological and chemical parameters from 05 October to 28 October 2018, when OH  
199 and HO<sub>2</sub> radicals were measured. The diurnal variations of the temperature (T), relative humidity (RH),  $j(\text{O}^1\text{D})$ , and  $j(\text{NO}_2)$   
200 followed a regular pattern from day to day. The overall meteorological conditions were characterized by high temperature  
201 (about 20–30 °C), high relative humidity (60–80%), and intensive radiation with  $j(\text{O}^1\text{D})$  up to  $2.0 \times 10^{-5} \text{ s}^{-1}$  and  $j(\text{NO}_2)$  up to  
202  $6.0 \times 10^{-3} \text{ s}^{-1}$ . The relative humidity and photolysis-frequency in this autumn campaign were similar to those in the summer  
203 campaign conducted inat Chengdu site (Yang et al., 2021). The temperature in this campaign was lower than that inat-Chengdu  
204 site, but similar to that in the autumn campaign at-in Heshan site-located in PRD as well (Tan et al., 2019;Yang et al., 2021).

205 The concentration of CO showed a weak diurnal variation, indicating there was the non-obvious accumulation of  
206 anthropogenic emissions on a regional scale. NO concentration peaked at 12 ppb during morning rush hour when the traffic  
207 emission was severe, and thereafter, O<sub>3</sub> concentration started to increase with the decreasing of NO concentration. The maxima  
208 of O<sub>3</sub> hourly concentration were high up to 120 ppb. According to the updated National Ambient Air Quality Standard of China  
209 (GB3095-2012), O<sub>3</sub> concentration exceeded the Class-II limit values (hourly averaged limit 93 ppb) on several days (6, 7, 8,  
210 and 26 October) when the environmental condition was characterized by high temperature and low relative humidity. NO<sub>2</sub>  
211 concentration was high at night because of the titration effect of O<sub>3</sub> with NO.

212 Along with the high O<sub>3</sub> concentration on 6, 7, 8, and 26 October, high HCHO concentration was also recorded during the  
213 corresponding periods, indicating HCHO was mainly produced as secondary pollutions because of the active photochemistry



214 in this campaign. Isoprene, which is mostly derived from biogenic emissions and mainly affected by temperature, peaked  
 215 around noontime. Tan et al. (2019) reported the median concentration of HCHO and isoprene concentrations were 6.8 ppb and  
 216 0.6 ppb during 12:00-18:00 at Heshan site. Similarly, the median concentration of HCHO and isoprene concentrations in this  
 217 study were 4.9 ppb and 0.4 ppb during the corresponding periods, respectively. As a proxy for traffic intensity, the toluene to  
 218 benzene ratio (T/B), which is below 2, means the traffic emissions are the major sources of VOCs (Brocco et al., 1997). In this  
 219 campaign, the T/B gradually dropped from 07:00 until it reached the minimum value at 09:00, indicating traffic emission  
 220 contributed more to VOCs during morning rush hour than during other periods. However, the T/B values, which varied within  
 221 a range of 7-12, was/were above 2, and thus VOCs emission during this campaign was mainly from other sectors such as those  
 222 involving solvent evaporation.



223  
 224 **Figure 2: Timeseries and diurnal profiles of the observed meteorological and chemical parameters in STORM campaign. The grey**  
 225 **areas denote nighttime.**

226 Moreover, we compared the environmental conditions between the Backgarden (rural site), Heshan (suburban site), and  
 227 Shenzhen (urban site) campaigns conducted in PRD in Table S3 in the Supplementary Information. No significant discrepancy  
 228 in temperature was found in the Shenzhen and Heshan campaigns, which were both conducted in autumn. The temperature in

带格式的: 行距: 1.5 倍行距

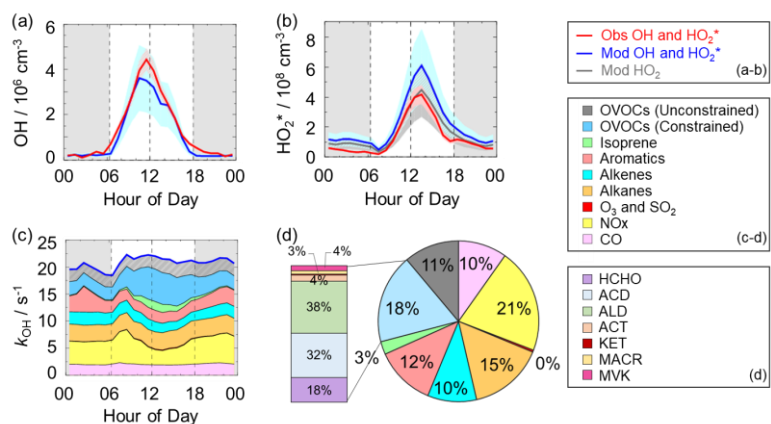
229 the Backgarden campaign conducted in summer was higher than those in Shenzhen and Heshan. The relative humidity in  
230 Shenzhen and Backgarden was higher than that in Heshan. Compared to the chemical conditions in the Heshan campaign  
231 conducted in autumn as well, the concentrations of CO, NO, NO<sub>2</sub>, HONO, alkenes, aromatics, and HCHO in Shenzhen were  
232 lower, which might be because there were no significant local pollution sources nearby ~~in~~at the Shenzhen site although it was  
233 an urban site. However, the concentration of O<sub>3</sub> which is the typical secondary pollutant in Shenzhen was higher than that in  
234 Heshan. Compared to the environmental conditions in Heshan, the higher O<sub>3</sub> concentration in Shenzhen might benefit from  
235 the weather condition which was characterized by the stronger solar radiation and slightly higher temperatures.

### 236 3.2 Observed and modeled OH and HO<sub>2</sub> radicals

237 The OH and HO<sub>2</sub> radicals were measured during 05-28 October 2018. The timeseries of the observed and modeled HOx  
238 concentrations are displayed in Fig. S42 (a-b) in the Supplementary Information. Data gaps were caused by the rain, calibration,  
239 and maintenance. The daily maxima of the observed OH and HO<sub>2</sub><sup>\*</sup> concentrations varied in the range of (2-9) × 10<sup>6</sup> cm<sup>-3</sup> and  
240 (2-14) × 10<sup>8</sup> cm<sup>-3</sup>, respectively. As in previous campaigns, the largest OH concentrations appeared around noontime and  
241 showed a high correlation with j(O<sup>1</sup>D), a proxy for the solar UV radiation driving much of the primary radical production (Tan  
242 et al., 2019).

243 Figure 3 (a-b) shows the diurnal profiles of the observed and modeled HOx concentrations. The HOx radicals showed similar  
244 diurnal behavior to those reported in other campaigns (Ma et al., 2019a; Tan et al., 2017; Tan et al., 2019; Tan et al., 2018; Yang  
245 et al., 2021). The observed OH and HO<sub>2</sub><sup>\*</sup> concentrations reached a maximum around 12:00 and 13:30, respectively. The  
246 diurnal maxima of the observed and modeled OH concentrations were 4.5 × 10<sup>6</sup> cm<sup>-3</sup> and 3.5 × 10<sup>6</sup> cm<sup>-3</sup>. Compared to the  
247 other campaigns conducted in PRD (Backgarden and Heshan), the diurnal maximum of the observed OH concentration in  
248 Shenzhen was equal to that observed in Heshan, and much lower than that observed in Backgarden where the observed OH  
249 concentration was nearly 15 × 10<sup>6</sup> cm<sup>-3</sup> (Hofzumahaus et al., 2009; Tan et al., 2019). The higher OH concentration ~~in~~at  
250 Backgarden site was closely correlated to the stronger solar radiation, as shown in Table S3 in the Supplementary Information.  
251 The diurnal observed and modeled OH concentrations agreed within their 1-σ uncertainties of measurement and simulation  
252 (11% and 40%). However, when the NO mixing ratio (Fig. 2) dropped from 10:00 gradually, a systematic difference existed,  
253 with the observed OH concentration being about 1 × 10<sup>6</sup> cm<sup>-3</sup> higher than the modeled OH concentration. The OH  
254 concentrations observed in the environments with low NO levels were underestimated by the state-of-the-art models at  
255 Backgarden (summer) and Heshan (autumn) sites in PRD as well, and the OH underestimation was identified to be universal  
256 at low NO conditions in China (Lu et al., 2013; Lu et al., 2012; Ma et al., 2019a; Tan et al., 2017; Yang et al., 2021; Ma et al.,  
257 2022b). The reasons on OH underestimation was further discussed in Section 4.1.

258



259

260

261

262

263

264

265

**Figure 3: (a-b) The diurnal profiles of the observed and modeled OH, HO<sub>2</sub>\* and HO<sub>2</sub> concentrations. (c) The diurnal profiles of the modeled  $k_{\text{OH}}$ . (d) The composition of the modeled  $k_{\text{OH}}$ . The red areas in (a-b) denote 1- $\sigma$  uncertainties of the observed OH and HO<sub>2</sub>\* concentrations. The blue areas in (a-b) denote 1- $\sigma$  uncertainties of the modeled OH and HO<sub>2</sub>\* concentrations, and the dark grey area in (b) denotes 1- $\sigma$  uncertainties of the modeled HO<sub>2</sub> concentrations. The grey areas in (a-c) denote nighttime. ACD denotes acetaldehydes, ALD denotes the C3 and higher aldehydes, ACT and KET denote acetone and ketones. MACR and MVK denote methacrolein and methyl vinyl ketone.**

266

267

268

269

270

271

272

273

274

275

276

277

278

279

The diurnal maximum of the observed HO<sub>2</sub>\*, the modeled HO<sub>2</sub>\* and the modeled HO<sub>2</sub> concentrations were  $4.2 \times 10^8 \text{ cm}^{-3}$ ,  $6.1 \times 10^8 \text{ cm}^{-3}$ , and  $4.4 \times 10^8 \text{ cm}^{-3}$ , respectively. The difference between the modeled HO<sub>2</sub>\* and HO<sub>2</sub> concentrations can be considered a modeled HO<sub>2</sub> interference from RO<sub>2</sub> (Lu et al., 2012). The RO<sub>2</sub> interference was small in the morning, while it became larger in the afternoon. It ranged within 23%-28% during the daytime (08:00-17:00), which was comparable with those ~~in-at~~ the Backgarden and Yufa sites in China, Borneo rainforest in Malaysia (OP3 campaign, aircraft), and UK (RONOCO campaign, aircraft) (Lu et al., 2012; Lu et al., 2013; Jones et al., 2011; Stone et al., 2014). The observed HO<sub>2</sub>\* was overestimated by the model, indicating the HO<sub>2</sub> heterogeneous uptake might have a significant impact during this campaign. The diurnal maximum of HO<sub>2</sub>\* concentration observed in Shenzhen was much lower than those observed ~~in-at~~ the Yufa and Backgarden sites (Hofzumahaus et al., 2009; Lu et al., 2012; Lu et al., 2013). The high modeled HO<sub>2</sub>\*/OH ratio around noontime (11:00-15:00), which was about 138, was found in this campaign, which was higher than those ~~in-at~~ the Backgarden and Chengdu sites (Yang et al., 2021; Hofzumahaus et al., 2009). High HO<sub>2</sub>\*/OH ratio is normally found only in clean air at low concentrations of NO<sub>x</sub> (Hofzumahaus et al., 2009; Stevens et al., 1997). As an indicator that can reflect the interconversion reaction between HO<sub>2</sub> and OH, the conversion efficiency in this campaign was slightly slower than ~~that-those in-at~~ the Backgarden and Chengdu sites.

280

### 3.3 OH reactivity

281

$k_{\text{OH}}$  is the pseudo-first-order loss rate coefficient of OH radicals, and it is equivalent to the reciprocal OH lifetime (Fuchs et

282 al., 2017; Lou et al., 2010; Yang et al., 2019). In this campaign,  $k_{\text{OH}}$  was measured only for several days (05-19 October 2018)  
283 by the LIP-LIF system, which has been reported in the previous study (Liu et al., 2019). The timeseries of the observed and  
284 modeled  $k_{\text{OH}}$  during 05-19 October 2018 are presented in Fig. S2-S3 in the Supplementary Information. A good agreement  
285 between the observed  $k_{\text{OH}}$  and modeled  $k_{\text{OH}}$  within the uncertainties was achieved, and thus the model can be believed to  
286 reproduce the observed  $k_{\text{OH}}$  values within the whole campaign. Moreover, to reflect the  $k_{\text{OH}}$  in the whole campaign, the modeled  
287 values were shown in the  $k_{\text{OH}}$  diurnal profiles (Fig. 3 (c)) and  $k_{\text{OH}}$  timeseries (Fig. S2 (c)) during 05-28 October 2018. The  
288 modeled  $k_{\text{OH}}$  showed a weak diurnal variation and varied from  $18 \text{ s}^{-1}$  to  $22 \text{ s}^{-1}$ . Compared to the  $k_{\text{OH}}$  variation in Shenzhen, the  
289  $k_{\text{OH}}$  observed in Backgarden and Heshan sites in PRD showed a stronger diurnal variation, with a minimum value at around  
290 noontime and a maximum value at daybreak. Additionally, the  $k_{\text{OH}}$  values in this campaign were lower than those at the  $k_{\text{OH}}$   
291 ranges in Backgarden ( $20\text{-}50 \text{ s}^{-1}$ ) and Heshan ( $22\text{-}32 \text{ s}^{-1}$ ) sites were  $20\text{-}50 \text{ s}^{-1}$  and  $22\text{-}32 \text{ s}^{-1}$  (Lou et al., 2010; Tan et al., 2019).  
292 Similar with the good agreement between the observed and modeled  $k_{\text{OH}}$  during the several days in Shenzhen, the observed  
293  $k_{\text{OH}}$  in Backgarden was matched well with the modeled  $k_{\text{OH}}$  which has included the OVOCs reactivity. In terms of the  $k_{\text{OH}}$  in  
294 Heshan, Tan et al. (2019) reported that only half of the observed  $k_{\text{OH}}$  was explained by the calculated  $k_{\text{OH}}$  which was calculated  
295 from the measured trace gas concentrations. The missing  $k_{\text{OH}}$  in Heshan was likely caused by unmeasured VOCs,  
296 demonstrating the necessary to measure more abundant VOCs species, especially OVOCs species.

297 As shown in Fig. 3 (d), we presented the composition of modeled  $k_{\text{OH}}$ . The inorganic compounds contributed approximately  
298 31% to  $k_{\text{OH}}$ , in which the CO and NO<sub>x</sub> reactivity accounted for 10% and 21%, respectively. The NO<sub>x</sub> reactivity was displayed  
299 versus time, with a maximum during the morning peak. The peak concentration during the morning peak was associated with  
300 traffic emissions.

301 Compared with the inorganics reactivity, the larger fraction of  $k_{\text{OH}}$  came from the VOCs group, with a contribution of 69%  
302 to  $k_{\text{OH}}$ . The contribution of alkanes, alkenes, and aromatics were 15%, 10%, and 12%, respectively. The isoprene reactivity  
303 related to temperature was mainly concentrated during the daytime, whereas the aromatics reactivity at night was higher. As  
304 for the OVOCs species, we measured several OVOCs species, including HCHO, acetaldehydes (ACD) and higher aldehydes  
305 (ALD), acetone (ACT), ketones (KET) and isoprene oxidation products (methacrolein (MACR) and methyl vinyl ketone  
306 (MVK)), so and thus we constrained these species in the model. The constrained OVOCs species accounted for 18% in the  
307 total  $k_{\text{OH}}$ , where HCHO, ACD, and ALD were the major contributors, with contributions of 18%, 32%, and 38% to the  
308 constrained OVOCs, respectively. The contribution of aldehydes in this study (16%) was larger than that in Beijing (Whalley  
309 et al., 2021) and smaller with that in Wangdu (Fuchs et al., 2017). The remaining reactivity was attributed to the unconstrained  
310 OVOCs reactivity, which came from the model-generated intermediate species (glyoxal, methylglyoxal, methyl ethyl ketone,  
311 methanol, etc.), with a contribution of 11% to the total  $k_{\text{OH}}$ . Large fraction of OVOCs reactivities in  $k_{\text{OH}}$  was also found in  
312 some previous studies (Lou et al., 2010; Lu et al., 2013; Fuchs et al., 2017; Whalley et al., 2021). About 50% of  $k_{\text{OH}}$  was  
313 explained by OVOCs at Backgarden site, and HCHO, ACD and ALD, and oxygenated isoprene products were the most

带格式的: 字体: 倾斜

带格式的: 下标

带格式的: 字体: 倾斜

带格式的: 下标

314 important OH reactants in OVOCs, with a contribution of 30-40%, and other 10-20% came from other oxygenated compounds  
315 (ketones, dicarbonyl compounds, alcohols, hydroperoxides, nitrates etc.) (Lou et al., 2010). HCHO, ACD, MVK, MVCR and  
316 glyoxal accounted for one-third of the total  $k_{OH}$  ~~in at~~ Wangdu site (Fuchs et al., 2017). The large unconstrained OVOCs  
317 reactivity indicated it is necessary to measure more VOCs species in the future.

## 318 4. Discussion

### 319 4.1 Radical closure experiment

320 In this study, we conducted OH radical closure experiment which is called OH experimental budget as well. As discussed in  
321 Section 3.3, it is believed that the model can reproduce the observed  $k_{OH}$ . Herein, to conduct the OH experiment budget in the  
322 whole campaign, we used the modeled  $k_{OH}$  to calculate the OH destruction rate because the  $k_{OH}$  was only measured on several  
323 days. The diurnal profiles of OH production and destruction rates, and the compositions of OH production rate were displayed  
324 in Fig. 4, with maxima of 14 ppb h<sup>-1</sup> and 17 ppb h<sup>-1</sup> around noontime, respectively. The OH production rate from known sources  
325 is quantified from the primary sources (photolysis of HONO, photolysis of O<sub>3</sub>, ozonolysis of alkenes) and secondary sources  
326 (dominated by HO<sub>2</sub> + NO, and HO<sub>2</sub> + O<sub>3</sub>). The primary and secondary sources ~~were-accounted~~ for 78% and 22% of the total  
327 calculated production rate, respectively. Similar with the prior studies, the largest fraction of OH production rate ~~eomes-came~~  
328 from HO<sub>2</sub> + NO, with a contribution up to 76% of the known OH production rate. ~~As the major primary OH sources, The~~  
329 ~~contributions-ofthe~~ HONO and O<sub>3</sub> photolysis ~~were-contributed~~ 13% and 7% to the ~~primary-total calculated OH~~ production rate,  
330 ~~respectively.~~

331 The OH production rate matched well with the destruction rate only in the early morning to about 10:00. Thereafter, the OH  
332 destruction rate was larger than the production rate, which could explain the underestimation of OH concentration by the model.  
333 ~~As shown in Fig. 4 (b), t~~he discrepancy between the OH production and destruction rates ~~at around 11:00-15:00in the~~  
334 ~~afternoon, which was approximately of (3.1~4.6) ppb h<sup>-1</sup>, cannot be explained by the combined experimental uncertainties.~~  
335 The discrepancy was attributed to the missing OH sources ~~because  $k_{OH}$  was constrained in this study~~. The biggest additional  
336 OH source was approximately 4.6 ppb h<sup>-1</sup>, which occurred at about 12:00, when the OH production and destruction rates were  
337 11.9 ppb h<sup>-1</sup> and 16.5 ppb h<sup>-1</sup>, respectively. The unknown OH source accounted for about one third of the total OH production  
338 rate, indicating the exploration of missing OH source was significant to study the radical chemistry. It is noted that the OH  
339 production rate was overestimated because we used HO<sub>2</sub> concentrations instead of HO<sub>2</sub> concentrations here. Thus, the  
340 missing OH source was the lower limit here, demonstrating more unknown OH sources need to be further explored. Details  
341 on unknown OH sources are given below (Sect. 4.2).

342

带格式的: 两端对齐, 缩进: 首行缩进: 1 字符, 段落间距段前: 6 磅

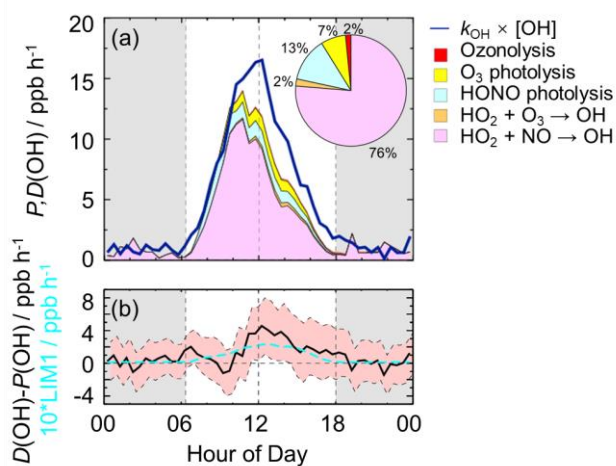
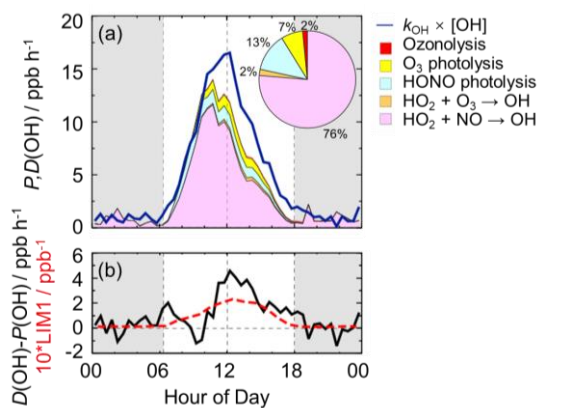


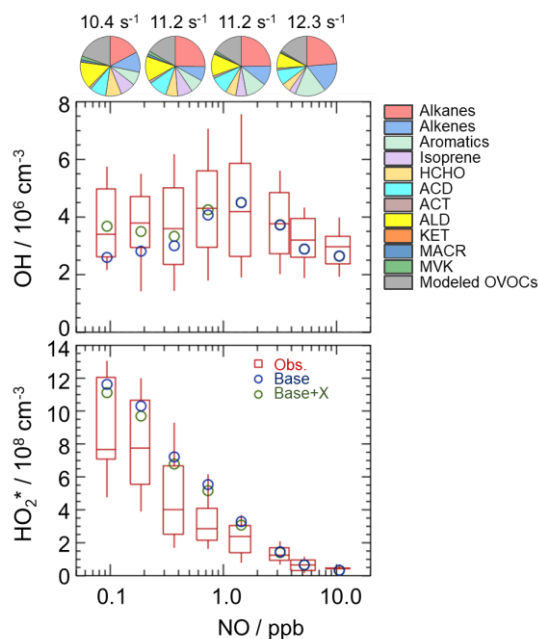
Figure 4: (a) The diurnal profiles of OH production and destruction rates and the proportions of different known sources in the calculated production rate during the daytime. The blue line denotes the OH destruction rate, and the colored areas denote the calculated OH production rates from the known sources. (b) The missing OH source which was the discrepancy between the OH destruction and production rates, and the OH production rate which was ten times the production rate derived from LIM1 mechanism. The red shaded areas denote the combined uncertainty from the experimental errors of the measured quantities (Table S1) and the reaction rate coefficients. The grey areas denote nighttime.

## 4.2 Radical chemistry in low NO regime

### 4.2.1 Influencing factors of OH underestimation

As analyzed in Sect. 4.1, the underestimation of OH concentration was attributable to the missing OH source. It is necessary to explore the influencing factor for gaining further insight into the missing source. Scientists reported that more significant OH underestimation would appear with the decreasing NO concentration and increasing isoprene concentration (Lu et al., 2012; Ren et al., 2008; Hofzumahaus et al., 2009; Lelieveld et al., 2008; Whalley et al., 2011; Tan et al., 2017; Yang et al., 2021).

357 Herein, we further explored the effect of NO concentration on missing OH source. The NO dependence of observed and  
 358 modeled HOx concentrations and the NO dependence on HOx observed-to-modeled ratios were OH and HO<sub>2</sub> radicals was  
 359 illustrated in Fig. 5 and Fig. S4. The OH concentrations were normalized by the averaged  $j(O^1D)$  to eliminate the influence of  
 360 radiation on radicals. The OH concentration showed an increasing trend with the increase of NO concentrations in low NO  
 361 regime (below 1 ppb) due to the increased OH radicals from propagation via peroxy reactions with NO, and then decreased  
 362 with the increase of NO concentrations in high NO regime (above 1 ppb) due to the OH loss by the reactions of OH with via  
 363 NO<sub>2</sub> (Ehhalt, 1999). The base model can reproduce the observed OH concentration in high NO regime and underestimate OH  
 364 concentration in low NO regime. As for HO<sub>2</sub>\* radicals, the observed and modeled HO<sub>2</sub>\* concentrations decreased with the  
 365 increase of NO concentrations. The model overestimated the observations, indicating the heterogeneous uptake might make a  
 366 significant role in HO<sub>2</sub> sinks in this campaign. Overall, NOx (= NO + NO<sub>2</sub>) plays a crucial role in radical chemistry due to the  
 367 impact of NO on radical propagation and termination reactions.



368 Figure 5: NO dependence of OH and HO<sub>2</sub>\* radicals. The red box-whisker plots give the 10%, 25%, median, 75%, and 90% of the  
 369 HOx observations. The blue circles show the median values of the HOx simulations by the base model, and the green circles show  
 370 the HOx simulations by the model with X mechanism. Total VOCs reactivity and their organic speciation are presented by pie charts  
 371 at the different NO intervals at the top. Only daytime values and NO concentration above the detection limit of the instrument were  
 372 chosen. ACD and ACT denote acetaldehyde and acetone, respectively. ALD denotes the C3 and higher aldehydes. KET denotes  
 373 ketones. MACR and MVK, which are both the isoprene oxidation products, denote methacrolein and methyl vinyl ketone,  
 374 respectively.  
 375

376 To further explore the influencing factors of OH underestimation, we presented the speciation VOCs reactivity under the

带格式的: 字体: 10 磅

带格式的: 字体: 10 磅

377 different NO intervals, as shown in Fig. 5 and Table S4 in the Supplementary Information. The isoprene reactivity and total  
378 OVOCs reactivity (the sum of HCHO, ACD, ACT, ALD, KET, MACR, MVK and the modeled OVOCs) increased with the  
379 decrease of NO concentrations, while the anthropogenic VOCs reactivity (alkanes, alkenes and aromatics) was higher in high  
380 NO regime. Additionally, the O<sub>3</sub> concentration in low NO regime was significantly higher than those in high NO regime, and  
381 the temperature was slightly higher in low NO regime, demonstrating the photochemistry was more active in low NO regime  
382 in this campaign. Overall, the photochemistry and composition of VOCs reactivity, especially the isoprene and OVOCs species  
383 (mainly [HCHO](#), [ACD](#), [ACTALD](#) and the modeled OVOCs), might closely impact the missing OH sources.

#### 384 4.2.2 Quantification of missing OH sources

385 Hofzumahaus et al. (2009) proposed an existence of a pathway for the regeneration of OH independent of NO, including the  
386 conversions of RO<sub>2</sub> → HO<sub>2</sub> and HO<sub>2</sub> → OH by a numerical species called X. With a retrospective analysis, the unclassical  
387 OH recycling pathway was identified to be universal at low NO conditions in China. The amount of X varies with  
388 environmental conditions, and the X concentrations were 0.85 ppb, 0.4 ppb, 0.1 ppb, 0.4 ppb, [0.1](#) and 0.25 ppb at Backgarden,  
389 Yufa, Wangdu, Heshan, [Taizhou](#), and Chengdu sites (Hofzumahaus et al., 2009; Lu et al., 2012; Lu et al., 2013; Tan et al.,  
390 2017; Yang et al., 2021; Ma et al., 2022b).

391 In this study, we tested this unclassical X mechanism. Good agreement between observations and simulations of OH radicals  
392 was achieved when a constant mixing ratio of 0.1 ppb of X was added into the base model. As shown in Fig. 5, the model with  
393 X mechanism agreed with the observed OH concentrations even at low NO conditions. Unclassical OH recycling was identified  
394 again in this study. However, X is an artificial species that behaves like NO, and thus the nature of X is still unknown to us.  
395 Compared to [the](#) Shenzhen site, the required X concentration in the Backgarden and Heshan sites in PRD ~~were was~~ higher,  
396 which might be affected by the different air masses in the three sites. The  $k_{OH}$  in Shenzhen site was much lower than those ~~at~~  
397 Backgarden and Heshan sites (Lu et al., 2013), and ~~the a~~ weaker diurnal variation of  $k_{OH}$  in Shenzhen was observed. Under the  
398 influence of the East Asian monsoon, the prevailing wind for PRD area is mostly southerly during the summer months and  
399 mostly northerly during the winter months (Fan et al., 2005; Zhang et al., 2008). The Backgarden site is located in Guangzhou,  
400 and the Heshan site is located in Jiangmen. The two cities are along the north-south axis, and thus the air masses of the  
401 Backgarden and Heshan sites are intimately linked with each other, while the air mass in Shenzhen is more similar to Hongkong  
402 (Zhang et al., 2008). [Compared to the VOCs reactivity in the air mass inat Backgarden and Yufa sites reported by Lu et al.](#)  
403 [\(2013\), lower isoprene reactivity and OVOCs reactivity were observed in Shenzhen site. As discussed in Section 4.2.1, the OH](#)  
404 [underestimation might be closely related to the composition of VOCs reactivity.](#) Therefore, further exploration ~~on of~~ this  
405 unclassical OH recycling is needed to improve our understanding of radical chemistry, [especially the mechanisms related to](#)  
406 [isoprene and OVOCs.](#)

407 As ~~for the~~ discussed in Section 4.2.1, ~~isoprene and OVOCs might have~~ potential influence of ~~isoprene and OVOCs~~ on the



408 missing OH sources, RO<sub>2</sub> isomerization reactions have also been shown to be of importance for the atmospheric fate of RO<sub>2</sub>  
409 from isoprene (Peeters et al., 2009; Peeters et al., 2014). The latest isoprene isomerization mechanism, which is called LIM1,  
410 has been coupled into our current base model. However, LIM1 mechanism was not included in the OH experimental budget  
411 which was conducted with the observations constrained, as shown in Section 4.1. Herein, we evaluated the contribution of  
412 LIM1 mechanism to the missing OH sources, as shown in Fig. 4 (b). LIM1 mechanism can explain approximately 7% of the  
413 missing OH sources during 10:00-16:00, when the missing OH production rate and the OH production rate derived from LIM1  
414 mechanism were 2.47 ppb h<sup>-1</sup> and 0.17 ppb h<sup>-1</sup>, respectively.

415 Additionally, prior studies also reported that OH regeneration might be achieved from the oxidation of MACR and MVK,  
416 which are the major first-generated products of isoprene (Fuchs et al., 2018; Fuchs et al., 2014). As a potential explanation for  
417 the high OH concentration, the impacts of MACR and MVK oxidation were evaluated here. The modification of MACR  
418 oxidation scheme added the H-migration reactions of MACR oxidation products (Fuchs et al., 2014). The modification of  
419 MVK oxidation scheme added the reactions of MVK oxidation products with HO<sub>2</sub> radicals and the H-migration reactions of  
420 MVK oxidation products (Fuchs et al., 2018). As presented in Fig. S3-S5 in the Supplementary Information, no significant of  
421 the MACR and MVK oxidation schemes was found in this campaign.

422 Overall, a large part of missing OH sources was not explained by the isoprene chemistry. In the future, the impact of OVOCs  
423 species which was another potential OH source on missing OH sources need to be further evaluated.

#### 424 4.3 HO<sub>2</sub> heterogeneous uptake Sources and sinks of RO<sub>x</sub>

425 The HO<sub>2</sub> overestimation was identified by comparing the observed and modeled HO<sub>2</sub> concentrations in Sect. 3.2 and Sect.

426 4.2.1. The HO<sub>2</sub> heterogeneous uptake has been proposed to be a potential sink of HO<sub>2</sub> radicals, and thus could influence the  
427 radical chemistry and the formation of secondary pollution, especially in high-aerosol environments (Song et al., 2021; Song  
428 et al., 2022; Tan et al., 2020; Kanaya et al., 2000; Kanaya et al., 2007; Li et al., 2019). The impact of HO<sub>2</sub> uptake chemistry on  
429 radical concentration is different under different environmental conditions (Whalley et al., 2015; Mao et al., 2010; Li et al.,  
430 2019). To evaluate the contribution of HO<sub>2</sub> uptake chemistry to radical concentrations in this study, we coupled HO<sub>2</sub>  
431 heterogeneous uptake into the base model (RACM2-LIM1) and conducted three sensitivity experiments, as shown in R1 and  
432 Eq. (3).



$$434 k_{\text{HO}_2+\text{aerosol}} = \frac{\gamma \cdot \text{ASA} \cdot v_{\text{HO}_2}}{4} \quad (3) \text{Eq.1}$$

435 where ASA [μm<sup>2</sup> cm<sup>-3</sup>], which represents the aerosol surface area concentration, can be estimated by multiplying the mass  
436 concentration of PM<sub>2.5</sub> [μg m<sup>-3</sup>] by 20 here because there were no direct ASA observations in this campaign (Chen et al.,  
437 2019; Wang et al., 2017b).  $v_{\text{HO}_2}$ , which can be calculated by Eq. (4), refers to the mean molecular velocity of HO<sub>2</sub> with a unit

带格式的: 下标

带格式的: 缩进: 首行缩进: 0 字符

of  $\text{cm s}^{-1}$ .

$$v_{\text{HO}_2} = \sqrt{\frac{8 \cdot R \cdot T}{0.033 \cdot \pi}} \quad (4) \text{Eq. 2}$$

where  $T$  [K] and  $R$  [ $\text{J mol}^{-1} \text{K}^{-1}$ ] denote the ambient temperature and gas constant.  $\gamma$ , the  $\text{HO}_2$  effective uptake coefficient, parameterizes the influence of some processes (Tan et al., 2020).  $\gamma$  varies in the highly uncertain range of 0-1 (Song et al., 2022), and is the most critical parameter to impact  $\text{HO}_2$  uptake chemistry. Only several observations of  $\gamma$  have been reported (Taketani et al., 2012; Zhou et al., 2021; Zhou et al., 2020). The measured  $\gamma$  at the Mt. Tai site and Mt. Mang site were 0.13-0.34 and 0.09-0.40, respectively (Taketani et al., 2012). The average value of the measured  $\gamma$  was 0.24 in Kyoto, Japan in the summer of 2018 (Zhou et al., 2020). Zhou et al. (2021) reported the lower-limit values for median and average values of the measured  $\gamma$  were 0.19 and  $0.23 \pm 0.21$  in Yokohama, Japan in the summer of 2019. Additionally, Li et al. (2018) set 0.2 as the value of  $\gamma$  in the model, and Tan et al. (2020) calculated the  $\gamma$  of  $0.08 \pm 0.13$  by the analysis of the measured radical budget in Wangdu.

Here, we applied the two  $\gamma$  (0.2 and 0.08), which have been used in the model, to evaluate the impact of  $\text{HO}_2$  uptake on radical concentrations, as shown in Fig. 6. The modeled  $\text{HO}_2^*$  cannot match well with the observations when  $\gamma$  of 0.08 and 0.2 was set in the model. As the  $\gamma$  increased to approximately 0.3, good agreement between the modeled and observed  $\text{HO}_2^*$  concentration was achieved, demonstrating that the significant heterogeneous uptake might exist in this campaign.

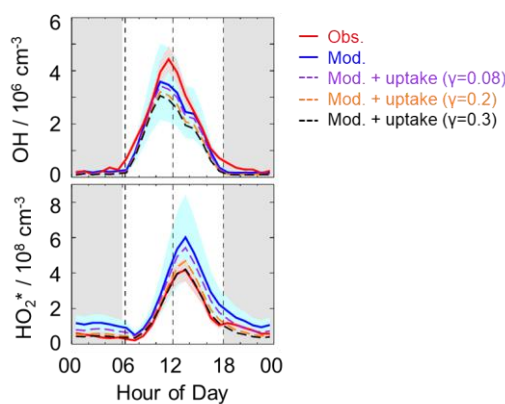


Figure 6: The diurnal profiles of the observed and modeled radical concentrations. The red and blue areas denote  $1-\sigma$  uncertainties of measured and simulated radical concentrations by the base model, respectively. The orange, purple and black lines denote the simulations by the model which added the  $\text{HO}_2$  heterogeneous uptake with different uptake coefficient. The grey areas denote nighttime.

It is noted that the estimated strong influence is speculative because of the uncertainties of measurements and simulations. Overall, the  $\gamma$  evaluated in this study was comparable with those observed at the Mt. Tai and Mt. Mang in China, and Kyoto

带格式的: 缩进: 首行缩进: 1 字符

带格式的: 居中

and Yokohama in Japan.

#### 4.4.3 Sources and sinks of ROx

The detailed analysis of radical sources and sinks was crucial to exploring radical chemistry. The experimental budget for HO<sub>2</sub> and RO<sub>2</sub> radicals could not be conducted because RO<sub>2</sub> was not measured during this campaign. Herein, we showed the simulated results by the base model. Figure 6-7 illustrates the diurnal profiles of ROx primary production rate ( $P(\text{ROx})$ ) and termination rate ( $L(\text{ROx})$ ), and the contributions of different channels during the daytime.

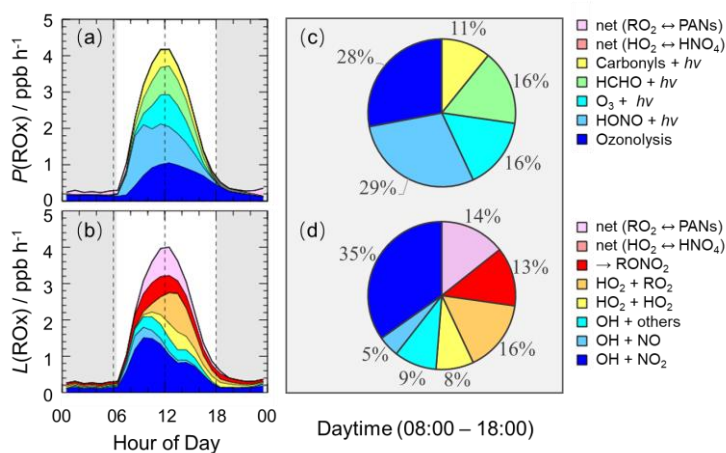


Figure 6-7: The diurnal profiles of ROx primary production rate (a) and termination rate (b) simulated by the base model, and the contributions of different channels to ROx primary production rate (c) and termination rate (d) during the daytime (08:00–18:00). The grey areas denote nighttime.

The ROx primary production and termination rates were basically in balance for the entire day, with maxima of 4  $\text{ppb h}^{-1}$  around noontime. The ROx primary production rate was similar to those at Heshan (4  $\text{ppb h}^{-1}$ ) and Wangdu (5  $\text{ppb h}^{-1}$ ) sites, but lower than those at Backgarden (11  $\text{ppb h}^{-1}$ ), Yufa (7  $\text{ppb h}^{-1}$ ), Taizhou (7  $\text{ppb h}^{-1}$ ) and Chengdu (7  $\text{ppb h}^{-1}$ ) sites (Lu et al., 2013; Lu et al., 2012; Tan et al., 2017; Tan et al., 2019; Yang et al., 2021). During the daytime, the  $P(\text{ROx})$  mainly came from the OH and HO<sub>2</sub> primary production. HONO and O<sub>3</sub> photolysis dominated the OH primary production, and HCHO photolysis dominated the HO<sub>2</sub> primary production. Thus,  $P(\text{ROx})$  was dominated by the photolysis reactions, in which the photolysis of HONO, O<sub>3</sub>, HCHO, and carbonyls accounted for 29%, 16%, 16%, and 11% during the daytime, respectively. In the early morning, HONO photolysis was the most important primary source of ROx, and the contribution of O<sub>3</sub> photolysis became progressively larger and was largest at noontime. A large discrepancy between the ratio of HONO photolysis rate to O<sub>3</sub> photolysis rate in summer/autumn and that in winter occurs generally. The vast majority of OH photolysis source is attributed to HONO photolysis in winter because of the higher HONO concentration and lower O<sub>3</sub> concentration. About half of  $L(\text{ROx})$

带格式的: 缩进: 首行缩进: 1 字符

带格式的: 上标

482 came from OH termination, which occurred mainly in the morning, and thereafter, radical self-combination gradually became  
 483 the major sink of ROx in the afternoon. OH + NO<sub>2</sub>, OH + NO, and OH + others contributed 35%, 5%, and 9% to *L*(ROx),  
 484 respectively. HO<sub>2</sub> + HO<sub>2</sub> and HO<sub>2</sub> + RO<sub>2</sub> accounted for 8% and 16% in *L*(ROx).

#### 485 4.5.4 AOC evaluation

486 AOC controls the abundance of precursors and the production of secondary pollutants (Yang et al., 2020a; Elshorbany et al.,  
 487 2009), and thus it is necessary to quantify AOC for understanding photochemical pollution. The AOC has been evaluated in  
 488 previous studies, as shown in Table 1. Overall, the AOC values in summer are higher than those in autumn and winter, and the  
 489 values at lower latitudes are higher than those at higher latitudes for the same season. The vast majority of AOC in previous  
 490 studies are evaluated based on the non-observed radical concentrations.

491 **Table 1: Summary of OH concentrations and AOC values reported in previous field campaigns.**

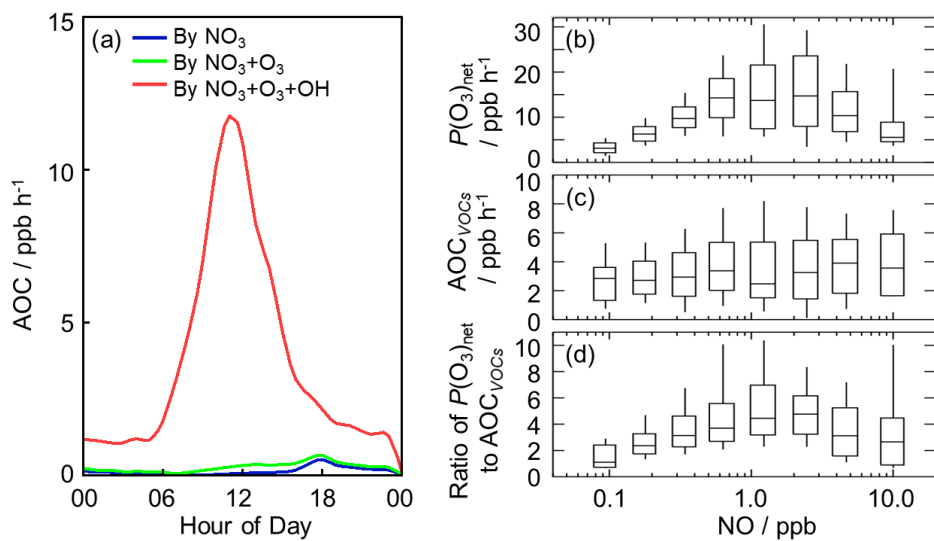
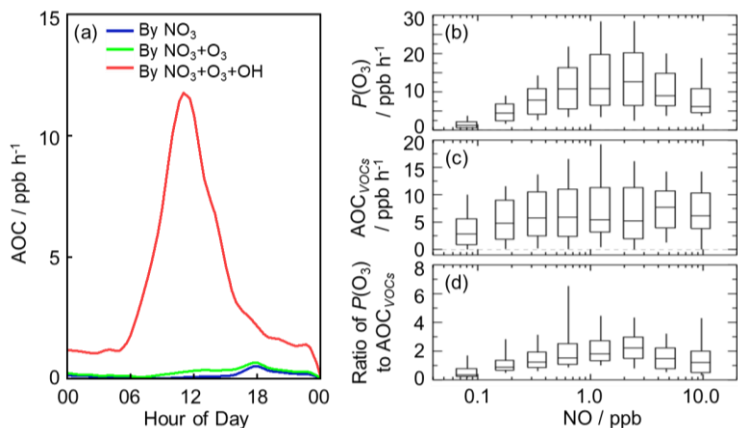
Location	Season, year	Site	Observed or non-	AOC / 10 <sup>8</sup>	References
			observed of OH radicals	molecules cm <sup>-3</sup> s <sup>-1</sup>	
Beijing, China	summer, 2018	urban	non-observed values	0.89 <sup>a</sup>	(Liu et al., 2021)
Beijing, China	summer, 2018	suburban	non-observed values	0.85 <sup>a</sup>	(Liu et al., 2021)
Beijing, China	winter, 2018	urban	non-observed values	0.21 <sup>a</sup>	(Liu et al., 2021)
Beijing, China	winter, 2018	suburban	non-observed values	0.16 <sup>a</sup>	(Liu et al., 2021)
Hongkong, China	summer, 2011	suburban	non-observed values	2.04 <sup>a,b</sup>	(Xue et al., 2016)
Santiago, Chile	summer, 2005	urban	non-observed values	3.4 <sup>a</sup>	(Elshorbany et al., 2009)
Hong Kong, China	late summer, 2012	coastal	non-observed values	1.4 <sup>c</sup>	(Li et al., 2018)
Hong Kong, China	autumn, 2012	coastal	non-observed values	0.62 <sup>c</sup>	(Li et al., 2018)
Hong Kong, China	winter, 2012	coastal	non-observed values	0.41 <sup>c</sup>	(Li et al., 2018)
Shanghai, China	summer, 2018	urban	non-observed values	1.0 <sup>e</sup>	(Zhu et al., 2020)
Berlin, Germany	summer, 1998	suburban	non-observed values	0.14 <sup>d</sup>	(Geyer et al., 2001)
Xianghe, China	autumn, 2019	suburban	non-observed values	0.49 <sup>e</sup>	(Yang et al., 2020a)
Beijing, China	summer, 2014	urban	non-observed values	1.7 <sup>a</sup>	(Feng et al., 2021)

492 Note that:

493 <sup>a</sup> Peak values in the diurnal profiles; <sup>b</sup> Values on 25 August 2021; <sup>c</sup> Maximum over a period of time; <sup>d</sup> Maximum on some day.

494 Herein, we explored the AOC in Shenzhen based on the observed radical concentrations for the first time. As illustrated in  
 495 Fig. 7-8 (a), the diurnal profile of AOC ~~exhibits~~-exhibited a unimodal pattern, which ~~is~~-was the same as the diurnal profile of  
 496 OH concentration and *j*(NO<sub>2</sub>), with a peak around noontime. The diurnal peak of AOC was 0.75 × 10<sup>8</sup> molecules cm<sup>-3</sup> s<sup>-1</sup> (11.8

497 ppb h<sup>-1</sup>). Comparatively, AOC in this study can be compared to those evaluated in Beijing (summer, 2018) and Hong  
 498 Kong (autumn, 2012) (Li et al., 2018; Liu et al., 2021), but much lower than those evaluated in Hong Kong (summer, 2011)  
 499 and Santiago (summer, 2005) (Xue et al., 2016; Elshorbany et al., 2009).



502 **Figure 78:** (a) The diurnal profiles of AOC in this campaign. (b) NO dependence of  $P(O_3)_{net}$  during the daytime. (c) NO  
 503 dependence of  $AOC_{VOCs}$  during the daytime, and  $AOC_{VOCs}$  denotes the atmospheric oxidation capacity only from the VOCs  
 504 oxidation. (d) NO dependence of the ratio of  $P(O_3)_{net}$  to  $AOC_{VOCs}$  during the daytime. The box-whisker plots in (b-d) give the 10%,  
 505 25%, median, 75%, and 90%  $P(O_3)_{net}$ ,  $AOC_{VOCs}$  and the ratio of  $P(O_3)_{net}$  to  $AOC_{VOCs}$ , respectively.

506 As expected, the dominant contributor to the AOC during this campaign was OH, followed by O<sub>3</sub> and NO<sub>3</sub>. Figure S4-S6  
 507 shows the fractional composition of the total AOC. The OH radical contributed about 95.7% of AOC during the daytime  
 508 (08:00-18:00). O<sub>3</sub>, as the second important oxidant, accounted for only 2.9% of AOC during the daytime. The contribution of

带格式的: 下标

带格式的: 下标

带格式的: 下标

带格式的: 下标

509 NO<sub>3</sub> to AOC during the daytime can be ignored, with a contribution of 1.4%. At night, the contributions of O<sub>3</sub> and NO<sub>3</sub> to  
510 AOC were higher. OH, O<sub>3</sub> and NO<sub>3</sub> accounted for 75.7%, 6.4%, and 18% in the first half of night (18:00-24:00), and they  
511 accounted for 87.8%, 5%, and 7.3% in the second half of night (00:00-08:00).

512 As the indicator for secondary pollution, net O<sub>3</sub> production rate,  $P(O_3)_{net}$ , can be calculated from the O<sub>3</sub> formation rate ( $F(O_3)$ )  
513 and the loss rate ( $L(O_3)$ ), as shown in Eq. (3-55-7) (Tan et al., 2017). The diurnal profiles of the speciation  $F(O_3)$  and  $L(O_3)$   
514 were shown in Fig. S5-S7 in the Supplementary Information. The diurnal maxima of the modeled  $F(O_3)$  and  $L(O_3)$  were 18.9  
515 ppb h<sup>-1</sup> and 2.8 ppb h<sup>-1</sup>, with the maximum  $P(O_3)_{net}$  of 16.1 ppb h<sup>-1</sup> at 11:00. ~~The modeled  $P(O_3)_{net}$  was comparable to that in~~  
516 ~~Wangdu site in summer and much higher than that in Beijing in winter (Tan et al., 2017; Tan et al., 2018).~~ ~~The modeled  $P(O_3)_{net}$~~   
517 ~~in this study was comparable to the net O<sub>3</sub> production rate in Wangdu site in summer (Tan et al., 2017), while it was much~~  
518 ~~higher than the O<sub>3</sub> production rate in Beijing in winter despite being the gross production rate (Tan et al., 2018).~~

$$519 F(O_3) = k_{HO_2+NO}[HO_2][NO] + \sum_i k_{RO_2+NO} [RO_2]_i [NO] \quad (35)$$

$$520 L(O_3) = \theta j(O^1D)[O_3] + k_{O_3+OH}[O_3][OH] + k_{O_3+HO_2}[O_3][HO_2] + (\sum(k_{alkenes+O_3}^i [alkenes^i]))[O_3] \quad (46)$$

$$521 P(O_3)_{net} = F(O_3) - L(O_3) - k_{NO_2+OH}[NO_2][OH]$$

$$522 (57)$$

523 where  $\theta$  is the fraction of O<sup>1</sup>D from ozone photolysis that reacts with water vapor.

524 Herein, we presented the NO dependence of  $P(O_3)_{net}$ ,  $AOC_{VOCs}$ , and the ratio of  $P(O_3)_{net}$  to  $AOC_{VOCs}$  in Fig. 7-8 (b-d), in  
525 which  $AOC_{VOCs}$  denotes the atmospheric oxidation capacity only from the VOCs oxidation, which includes the channels of  
526 primary VOCs (excluding OVOCS, and mainly alkanes, alkenes, aromatics and isoprene) with OH radicals. An upward trend  
527 of  $P(O_3)_{net}$  was presented with the increase of NO concentration when NO concentration was below 1 ppb, while  $P(O_3)_{net}$   
528 decreased with the increase of NO concentration because NO<sub>2</sub> became the sink of OH radicals gradually. ~~a downward trend was~~  
529 ~~shown with the increase of NO concentration~~ when NO concentration was above 1 ppb. In terms of the NO dependence of  
530  $AOC_{VOCs}$ , no significant variation was found, indicating VOCs oxidation was weakly impacted by NO concentrations in this  
531 campaign. Since  $AOC_{VOCs}$  can represent the VOCs oxidant rate, and thus the ratio of  $P(O_3)_{net}$  to  $AOC_{VOCs}$  can reflect the yield  
532 of net ozone production from VOCs oxidation. Similar to  $P(O_3)_{net}$ , the ratios increased with the increase of NO concentration  
533 when NO concentration was below 1 ppb, while ~~When NO concentration was above 1 ppb,~~ the ratios decreased with the  
534 increase of NO concentration when NO concentration was above 1 ppb, indicating the yield of net O<sub>3</sub> production from VOCs  
535 oxidation would be lower within the low NO regime (< 1 ppb) and high NO regime (> 1 ppb). The median ratios ranged from  
536 1.0 to 4.5, and the maximum of the median ratios existed when NO concentration was approximately 1 ppb, with a median value  
537 of approximately 4.5. The nonlinear response of the yield of net ozone production from VOCs oxidation to NO indicated that  
538 it is necessary to optimize the NO<sub>x</sub> and VOC control strategies for the reduction of O<sub>3</sub> pollution effectively, because NO<sub>2</sub>  
539 became the sink of OH radicals gradually. The maximum of the ratios existed when NO concentration was approximately 1

带格式的: 下标

带格式的: 下标

带格式的: 字体: 10 磅

带格式的: 字体: 10 磅

带格式的: 字体: 10 磅

带格式的: 字体: 10 磅

带格式的: 字体: 10 磅

带格式的: 字体: 10 磅

带格式的: 字体: 10 磅

带格式的: 下标

带格式的: 下标

带格式的: 下标

带格式的: 下标

带格式的: 下标

540 ppb, with a median of about 2, indicating the yield of ozone production from VOCs oxidation was about 2 in this study.

## 542 5 Conclusions

543 The STORM field campaign was carried out at Shenzhen site in the autumn of 2018, providing the continuous OH and HO<sub>2</sub>  
544 observations in PRD since the Heshan campaign in 2014. The maximum diurnal OH and HO<sub>2</sub> concentrations, which were  
545 measured by laser-induced fluorescence (LIF)PKU-LIF system, were  $4.5 \times 10^6 \text{ cm}^{-3}$  and 4.54.2  $\times 10^8 \text{ cm}^{-3}$ , respectively. The  
546 observed OH concentration was equal to that measured at Heshan site (autumn campaign) but was lower than those measured  
547 in summer campaigns in China (Backgarden, Yufa, Wangdu, Taizhou and Chengdu sites). The observed HO<sub>2</sub> concentrations  
548 included the true HO<sub>2</sub> concentrations and an estimated interference from RO<sub>2</sub> radicals, and was much lower than those  
549 measured at the Backgarden and Yufa sites in China.

550 The base model (RACM2-LIM1) could reproduce the observed OH concentration before 10:00, and thereafter, OH was  
551 underestimated by the model when NO concentration dropped to low levels. The results of the radical experimental budget  
552 indicated that OH underestimation was likely attributable to an unknown missing OH source at low NO conditionsregime. We  
553 diagnosed the missing OH source by sensitivity runs, and unclassical OH recycling was identified again in this study. Good  
554 agreement between the modeled and observed OH concentrations was achieved when a constant mixing ratio of the  
555 numerical species, X, equivalent to 0.1 ppb NO, was added into the base model to achieve the agreement between the modeled  
556 and observed OH concentrations. Additionally, we found isoprene and OVOCs might closely influence the missing OH sources  
557 by comparing the composition of VOCs reactivity under the different NO intervals. Isoprene isomerization mechanism (LIM1)  
558 can explain approximately 7% of the missing OH sourcesproduction rate, and no significant contribution of MACR and MVK  
559 oxidation was found. As another potential OH source, OVOCs species should be further explored to explain the remaining  
560 missing OH sources. As for HO<sub>2</sub> radicals, the overestimation of HO<sub>2</sub> concentration was found, indicating that HO<sub>2</sub>  
561 heterogeneous uptake with the effective uptake coefficient of 0.3 might make a significant role in HO<sub>2</sub> sinks.

562 The quantification of production and destruction channels of ROx radicals is essential to explore the chemical processes of  
563 radicals. The ROx primary production and termination rates were balanced for the entire day, with maxima of  $4 \text{ ppb h}^{-1}$ , similar  
564 to those in at the Heshan and Wangdu sites. Photolysis channels dominated the ROx primary production rate, and the HONO,  
565 O<sub>3</sub>, HCHO, and carbonyls photolysis accounted for 29%, 16%, 16%, and 11% during the daytime, respectively. The most  
566 fraction of ROx termination rate came from the reaction of OH + NO<sub>2</sub> in the morning. The radical self-combination gradually  
567 became the major sink of ROx in the afternoon with the decreasing of NO concentrations. The reaction of OH + NO<sub>2</sub> and  
568 radical self-combination accounted for 35% and 24% during the daytime, respectively.

569 In this campaign, AOC exhibited well-defined diurnal patterns, with a peak of  $11.8 \text{ ppb h}^{-1}$ . As expected, OH radicals, which

带格式的: 下标

带格式的: 缩进: 首行缩进: 1 字符

570 were the dominant oxidant, accounted for 95.7% of the total AOC during the daytime. O<sub>3</sub> and NO<sub>3</sub> contributed 2.9% and 1.4%  
571 to total AOC during the daytime, respectively. The ratio of  $P(\text{O}_3)_{\text{net}}$  to  $\text{AOC}_{\text{VOCs}}$ , which denotes the yield of net ozone  
572 production from VOCs oxidation, trended to increase and then decrease as NO concentration increased, with a range of 1.0-  
573 4.5, demonstrating the non-linear relationship between O<sub>3</sub> production and VOCs oxidation. Optimizing the NOx and VOCs  
574 control strategies might be significant to realize the reduction of ozone concentrations based on the nonlinear relationship  
575 between the yield of net ozone production from VOCs oxidation and NO concentrations. The maximum of the ratios existed  
576 when NO concentration was approximately 1 ppb, with a median of about 2, indicating that the yield of ozone production from  
577 VOCs oxidation was about 2 in this campaign.

带格式的: 下标

579 **Data availability.** The data used in this study are available from the corresponding author upon request (k.lu@pku.edu.cn).

580  
581 **Author contributions.** YH Zhang and KD Lu conceived the study. XP Yang analyzed the data and wrote the manuscript with  
582 inputs from KD Lu. XP Yang, XF Ma, Y Gao contributed to the measurements of the HOx concentrations. All authors  
583 contributed to the discussed results and commented on the manuscript.

584  
585 **Competing interests.** The authors declare that they have no conflict of interest.

586  
587 **Acknowledgment.** The authors thank the science teams of the STORM-2018 campaign. This work was supported by the  
588 Beijing Municipal Natural Science Foundation for Distinguished Young Scholars (JQ19031), the National Research Program  
589 for Key Issue in Air Pollution Control (2019YFC0214800), and the National Natural Science Foundation of China (Grants  
590 No. 91544225, 21522701, 91844301).

## 591 Appendix A. Supplementary data

## 592 References

- 593 Berndt, T., Chen, J., Kjaergaard, E. R., Moller, K. H., Tilgner, A., Hoffmann, E. H., Herrmann, H., Crouse, J. D., Wennberg,  
594 P. O., and Kjaergaard, H. G.: Hydrotrioxide (ROOOH) formation in the atmosphere, *Science*, 376, 979-+,  
595 10.1126/science.abn6012, 2022.
- 596 Brocco, D., Fratarcangeli, R., Lepore, L., Petricca, M., and Ventrone, I.: Determination of aromatic hydrocarbons in urban air  
597 of Rome, *Atmospheric Environment*, 31, 557-566, 10.1016/s1352-2310(96)00226-9, 1997.
- 598 Chen, X., Wang, H., Liu, Y., Su, R., Wang, H., Lou, S., and Lu, K.: Spatial characteristics of the nighttime oxidation capacity  
599 in the Yangtze River Delta, China, *Atmospheric Environment*, 208, 150-157, 10.1016/j.atmosenv.2019.04.012, 2019.
- 600 Ehhalt, D. H.: Photooxidation of trace gases in the troposphere, *Physical Chemistry Chemical Physics*, 1, 5401-5408,  
601 10.1039/a905097c, 1999.
- 602 Elshorbany, Y. F., Kurtenbach, R., Wiesen, P., Lissi, E., Rubio, M., Villena, G., Gramsch, E., Rickard, A. R., Pilling, M. J., and

域代码已更改

带格式的: 字体: (默认) Times New Roman



603 Kleffmann, J.: Oxidation capacity of the city air of Santiago, Chile, *Atmospheric Chemistry and Physics*, 9, 2257-2273,  
604 10.5194/acp-9-2257-2009, 2009.

605 Fan, S., Wang, A., Fan, Q., Liu, J., and Wang, B.: ATMOSPHERIC BOUNDARY LAYER CONCEPT MODEL OF THE  
606 PEARL RIVER DELTA AND ITS APPLICATION, *Journal of Tropical Meteorology*, 21, 286-292, 2005.

607 Feng, T., Zhao, S. Y., Hu, B., Bei, N. F., Zhang, X., Wu, J. R., Li, X., Liu, L., Wang, R. N., Tie, X. X., and Li, G. H.: Assessment  
608 of Atmospheric Oxidizing Capacity Over the Beijing-Tianjin-Hebei (BTH) Area, China, *Journal of Geophysical Research-  
609 Atmospheres*, 126, 18, 10.1029/2020jd033834, 2021.

610 Fittschen, C.: The reaction of peroxy radicals with OH radicals, *Chemical Physics Letters*, 725, 102-108,  
611 10.1016/j.cplett.2019.04.002, 2019.

612 Fittschen, C., Al Ajami, M., Batut, S., Ferracci, V., Archer-Nicholls, S., Archibald, A. T., and Schoemaeker, C.: ROOOH: a  
613 missing piece of the puzzle for OH measurements in low-NO environments?, *Atmospheric Chemistry and Physics*, 19, 349-  
614 362, 10.5194/acp-19-349-2019, 2019.

615 Fuchs, H., Holland, F., and Hofzumahaus, A.: Measurement of tropospheric RO<sub>2</sub> and HO<sub>2</sub> radicals by a laser-induced  
616 fluorescence instrument, *Review of Scientific Instruments*, 79, 10.1063/1.2968712, 2008.

617 Fuchs, H., Bohn, B., Hofzumahaus, A., Holland, F., Lu, K. D., Nehr, S., Rohrer, F., and Wahner, A.: Detection of HO<sub>2</sub> by laser-  
618 induced fluorescence: calibration and interferences from RO<sub>2</sub> radicals, *Atmospheric Measurement Techniques*, 4, 1209-1225,  
619 10.5194/amt-4-1209-2011, 2011.

620 Fuchs, H., Acir, I. H., Bohn, B., Brauers, T., Dorn, H. P., Häsel, R., Hofzumahaus, A., Holland, F., Kaminski, M., Li, X., Lu,  
621 K., Lutz, A., Nehr, S., Rohrer, F., Tillmann, R., Wegener, R., and Wahner, A.: OH regeneration from methacrolein oxidation  
622 investigated in the atmosphere simulation chamber SAPHIR, *Atmos. Chem. Phys.*, 14, 7895-7908, 10.5194/acp-14-7895-2014,  
623 2014.

624 Fuchs, H., Tan, Z., Hofzumahaus, A., Broch, S., Dorn, H.-P., Holland, F., Kuenstler, C., Gomm, S., Rohrer, F., Schrade, S.,  
625 Tillmann, R., and Wahner, A.: Investigation of potential interferences in the detection of atmospheric RO<sub>x</sub> radicals by laser-  
626 induced fluorescence under dark conditions, *Atmospheric Measurement Techniques*, 9, 1431-1447, 10.5194/amt-9-1431-2016,  
627 2016.

628 Fuchs, H., Tan, Z., Lu, K., Bohn, B., Broch, S., Brown, S. S., Dong, H., Gomm, S., Haeseler, R., He, L., Hofzumahaus, A.,  
629 Holland, F., Li, X., Liu, Y., Lu, S., Min, K.-E., Rohrer, F., Shao, M., Wang, B., Wang, M., Wu, Y., Zeng, L., Zhang, Y., Wahner,  
630 A., and Zhang, Y.: OH reactivity at a rural site (Wangdu) in the North China Plain: contributions from OH reactants and  
631 experimental OH budget, *Atmospheric Chemistry and Physics*, 17, 645-661, 10.5194/acp-17-645-2017, 2017.

632 Fuchs, H., Albrecht, S., Acir, I.-H., Bohn, B., Breitenlechner, M., Dorn, H.-P., Gkatzelis, G. I., Hofzumahaus, A., Holland, F.,  
633 Kaminski, M., Keutsch, F. N., Novelli, A., Reimer, D., Rohrer, F., Tillmann, R., Vereecken, L., Wegener, R., Zaytsev, A.,  
634 Kiendler-Scharr, A., and Wahner, A.: Investigation of the oxidation of methyl vinyl ketone (MVK) by OH radicals in the  
635 atmospheric simulation chamber SAPHIR, *Atmospheric Chemistry and Physics*, 18, 8001-8016, 10.5194/acp-18-8001-2018,  
636 2018.

637 Gao, M., Li, H., Li, Y., Wei, J., Sun, Y., He, L., and Huang, X.: Source characteristics of water-soluble organic matters in  
638 PM<sub>2.5</sub> in the winter of Shenzhen, *China Environmental Science*, 38, 4017-4022, 2018.

639 Geyer, A., Alicke, B., Konrad, S., Schmitz, T., Stutz, J., and Platt, U.: Chemistry and oxidation capacity of the nitrate radical  
640 in the continental boundary layer near Berlin, *Journal of Geophysical Research-Atmospheres*, 106, 8013-8025,  
641 10.1029/2000jd900681, 2001.

642 Heard, D. E., and Pilling, M. J.: Measurement of OH and HO<sub>2</sub> in the troposphere, *Chemical Reviews*, 103, 5163-5198,  
643 10.1021/cr020522s, 2003.

644 Hofzumahaus, A., Aschmutat, U., Hessling, M., Holland, F., and Ehhalt, D. H.: The measurement of tropospheric OH radicals  
645 by laser-induced fluorescence spectroscopy during the POPCORN field campaign, *Geophysical Research Letters*, 23, 2541-  
646 2544, 10.1029/96gl02205, 1996.

647 Hofzumahaus, A., Rohrer, F., Lu, K., Bohn, B., Brauers, T., Chang, C.-C., Fuchs, H., Holland, F., Kita, K., Kondo, Y., Li, X.,  
648 Lou, S., Shao, M., Zeng, L., Wahner, A., and Zhang, Y.: Amplified Trace Gas Removal in the Troposphere, *Science*, 324, 1702-  
649 1704, 10.1126/science.1164566, 2009.

650 Holland, F., Hessling, M., and Hofzumahaus, A.: IN-SITU MEASUREMENT OF TROPOSPHERIC OH RADICALS BY  
651 LASER-INDUCED FLUORESCENCE - A DESCRIPTION OF THE KFA INSTRUMENT, *Journal of the Atmospheric*  
652 *Sciences*, 52, 3393-3401, 10.1175/1520-0469(1995)052<3393:ismoto>2.0.Co;2, 1995.

653 Huang, X.-F., Chen, D.-L., Lan, Z.-J., Feng, N., He, L.-Y., Yu, G.-H., and Luan, S.-J.: Characterization of organic aerosol in  
654 fine particles in a mega-city of South China: Molecular composition, seasonal variation, and size distribution, *Atmospheric*  
655 *Research*, 114-115, 28-37, <https://doi.org/10.1016/j.atmosres.2012.05.019>, 2012a.

656 Huang, X.-F., Sun, T.-L., Zeng, L.-W., Yu, G.-H., and Luan, S.-J.: Black carbon aerosol characterization in a coastal city in  
657 South China using a single particle soot photometer, *Atmospheric Environment*, 51, 21-28,  
658 <https://doi.org/10.1016/j.atmosenv.2012.01.056>, 2012b.

659 Jones, C. E., Hopkins, J. R., and Lewis, A. C.: In situ measurements of isoprene and monoterpenes within a south-east Asian  
660 tropical rainforest, *Atmospheric Chemistry and Physics*, 11, 6971-6984, 10.5194/acp-11-6971-2011, 2011.

661 Kanaya, Y., Sadanaga, Y., Matsumoto, J., Sharma, U. K., Hirokawa, J., Kajii, Y., and Akimoto, H.: Daytime HO<sub>2</sub> concentrations  
662 at Oki Island, Japan, in summer 1998: Comparison between measurement and theory, *Journal of Geophysical Research-*  
663 *Atmospheres*, 105, 24205-24222, 10.1029/2000jd900308, 2000.

664 Kanaya, Y., Cao, R., Kato, S., Miyakawa, Y., Kajii, Y., Tanimoto, H., Yokouchi, Y., Mochida, M., Kawamura, K., and Akimoto,  
665 H.: Chemistry of OH and HO<sub>2</sub> radicals observed at Rishiri Island, Japan, in September 2003: Missing daytime sink of HO<sub>2</sub>  
666 and positive nighttime correlations with monoterpenes, *Journal of Geophysical Research-Atmospheres*, 112,  
667 10.1029/2006jd007987, 2007.

668 Lelieveld, J., Butler, T. M., Crowley, J. N., Dillon, T. J., Fischer, H., Ganzeveld, L., Harder, H., Lawrence, M. G., Martinez,  
669 M., Taraborrelli, D., and Williams, J.: Atmospheric oxidation capacity sustained by a tropical forest, *Nature*, 452, 737-740,  
670 10.1038/nature06870, 2008.

671 Levy, H.: NORMAL ATMOSPHERE - LARGE RADICAL AND FORMALDEHYDE CONCENTRATIONS PREDICTED,  
672 *Science*, 173, 141-&, 10.1126/science.173.3992.141, 1971.

673 Li, K., Jacob, D. J., Liao, H., Shen, L., Zhang, Q., and Bates, K. H.: Anthropogenic drivers of 2013-2017 trends in summer  
674 surface ozone in China, *Proceedings of the National Academy of Sciences of the United States of America*, 116, 422-427,  
675 10.1073/pnas.1812168116, 2019.

676 Li, Z., Xue, L., Yang, X., Zha, Q., Tham, Y. J., Yan, C., Louie, P. K. K., Luk, C. W. Y., Wang, T., and Wang, W.: Oxidizing  
677 capacity of the rural atmosphere in Hong Kong, Southern China, *Science of the Total Environment*, 612, 1114-1122,  
678 10.1016/j.scitotenv.2017.08.310, 2018.

679 Liu, S., Li, X., Shen, X., Zeng, L., Huang, X., Zhu, B., Lin, L., and Lou, S.: Measurement and partition analysis of atmospheric  
680 OH reactivity in autumn in Shenzhen, *Acta Scientiae Circumstantiae*, 39, 3600-3610, 2019.

681 Liu, Z., Wang, Y., Hu, B., Lu, K., Tang, G., Ji, D., Yang, X., Gao, W., Xie, Y., Liu, J., Yao, D., Yang, Y., and Zhang, Y.:  
682 Elucidating the quantitative characterization of atmospheric oxidation capacity in Beijing, China, *Science of the Total*  
683 *Environment*, 771, 10.1016/j.scitotenv.2021.145306, 2021.

684 Lou, S., Holland, F., Rohrer, F., Lu, K., Bohn, B., Brauers, T., Chang, C. C., Fuchs, H., Haeseler, R., Kita, K., Kondo, Y., Li,  
685 X., Shao, M., Zeng, L., Wahner, A., Zhang, Y., Wang, W., and Hofzumahaus, A.: Atmospheric OH reactivities in the Pearl  
686 River Delta - China in summer 2006: measurement and model results, *Atmospheric Chemistry and Physics*, 10, 11243-11260,  
687 10.5194/acp-10-11243-2010, 2010.

688 Lu, K., Guo, S., Tan, Z., Wang, H., Shang, D., Liu, Y., Li, X., Wu, Z., Hu, M., and Zhang, Y.: Exploring atmospheric free-  
689 radical chemistry in China: the self-cleansing capacity and the formation of secondary air pollution, *National Science Review*,  
690 6, 579-594, 10.1093/nsr/nwy073, 2019.

691 Lu, K. D., Rohrer, F., Holland, F., Fuchs, H., Bohn, B., Brauers, T., Chang, C. C., Haeseler, R., Hu, M., Kita, K., Kondo, Y.,  
692 Li, X., Lou, S. R., Nehr, S., Shao, M., Zeng, L. M., Wahner, A., Zhang, Y. H., and Hofzumahaus, A.: Observation and modelling  
693 of OH and HO<sub>2</sub> concentrations in the Pearl River Delta 2006: a missing OH source in a VOC rich atmosphere, *Atmospheric*  
694 *Chemistry and Physics*, 12, 1541-1569, 10.5194/acp-12-1541-2012, 2012.

695 Lu, K. D., Hofzumahaus, A., Holland, F., Bohn, B., Brauers, T., Fuchs, H., Hu, M., Haeseler, R., Kita, K., Kondo, Y., Li, X.,  
696 Lou, S. R., Oebel, A., Shao, M., Zeng, L. M., Wahner, A., Zhu, T., Zhang, Y. H., and Rohrer, F.: Missing OH source in a

带格式的: 字体: (默认) Times New Roman

带格式的: 字体: (默认) Times New Roman

带格式的: 字体: (默认) Times New Roman

带格式的: 字体: (默认) Times New Roman

697 suburban environment near Beijing: observed and modelled OH and HO<sub>2</sub> concentrations in summer 2006, *Atmospheric*  
698 *Chemistry and Physics*, 13, 1057-1080, 10.5194/acp-13-1057-2013, 2013.

699 Ma, X., Tan, Z., Lu, K., Yang, X., Liu, Y., Li, S., Li, X., Chen, S., Novelli, A., Cho, C., Zeng, L., Wahner, A., and Zhang, Y.:  
700 Winter photochemistry in Beijing: Observation and model simulation of OH and HO<sub>2</sub> radicals at an urban site, *Science of the*  
701 *Total Environment*, 685, 85-95, 10.1016/j.scitotenv.2019.05.329, 2019a.

702 Ma, X., Tan, Z., Lu, K., Yang, X., Chen, X., Wang, H., Chen, S., Fang, X., Li, S., Li, X., Liu, J., Liu, Y., Lou, S., Qiu, W.,  
703 Wang, H., Zeng, L., and Zhang, Y.: OH and HO<sub>2</sub> radical chemistry at a suburban site during the EXPLORE-YRD campaign  
704 in 2018, *Atmospheric Chemistry and Physics*, 22, 7005-7028, 10.5194/acp-22-7005-2022, 2022a.

705 Ma, X. F., Tan, Z. F., Lu, K. D., Yang, X. P., Chen, X. R., Wang, H. C., Chen, S. Y., Fang, X., Li, S. L., Li, X., Liu, J. W., Liu,  
706 Y., Lou, S. R., Qiu, W. Y., Wang, H. L., Zeng, L. M., and Zhang, Y. H.: OH and HO<sub>2</sub> radical chemistry at a suburban site during  
707 the EXPLORE-YRD campaign in 2018, *Atmospheric Chemistry and Physics*, 22, 7005-7028, 10.5194/acp-22-7005-2022,  
708 2022b.

709 Ma, X. Y., Jia, H. L., Sha, T., An, J. L., and Tian, R.: Spatial and seasonal characteristics of particulate matter and gaseous  
710 pollution in China: Implications for control policy, *Environmental Pollution*, 248, 421-428, 10.1016/j.envpol.2019.02.038,  
711 2019b.

712 Mao, J., Jacob, D. J., Evans, M. J., Olson, J. R., Ren, X., Brune, W. H., St Clair, J. M., Crounse, J. D., Spencer, K. M., Beaver,  
713 M. R., Wennberg, P. O., Cubison, M. J., Jimenez, J. L., Fried, A., Weibring, P., Walega, J. G., Hall, S. R., Weinheimer, A. J.,  
714 Cohen, R. C., Chen, G., Crawford, J. H., McNaughton, C., Clarke, A. D., Jaegle, L., Fisher, J. A., Yantosca, R. M., Le Sager,  
715 P., and Carouge, C.: Chemistry of hydrogen oxide radicals (HO<sub>x</sub>) in the Arctic troposphere in spring, *Atmospheric Chemistry*  
716 *and Physics*, 10, 5823-5838, 10.5194/acp-10-5823-2010, 2010.

717 Mao, J., Ren, X., Zhang, L., Van Duin, D. M., Cohen, R. C., Park, J. H., Goldstein, A. H., Paulot, F., Beaver, M. R., Crounse,  
718 J. D., Wennberg, P. O., DiGangi, J. P., Henry, S. B., Keutsch, F. N., Park, C., Schade, G. W., Wolfe, G. M., Thornton, J. A., and  
719 Brune, W. H.: Insights into hydroxyl measurements and atmospheric oxidation in a California forest, *Atmospheric Chemistry*  
720 *and Physics*, 12, 8009-8020, 10.5194/acp-12-8009-2012, 2012.

721 Novelli, A., Hens, K., Ernest, C. T., Kubistin, D., Regelin, E., Elste, T., Plass-Duelmer, C., Martinez, M., Lelieveld, J., and  
722 Harder, H.: Characterisation of an inlet pre-injector laser-induced fluorescence instrument for the measurement of atmospheric  
723 hydroxyl radicals, *Atmospheric Measurement Techniques*, 7, 3413-3430, 10.5194/amt-7-3413-2014, 2014.

724 Peeters, J., Nguyen, T. L., and Vereecken, L.: HO<sub>x</sub> radical regeneration in the oxidation of isoprene, *Physical Chemistry*  
725 *Chemical Physics*, 11, 5935-5939, 10.1039/b908511d, 2009.

726 Peeters, J., and Muller, J.-F.: HO<sub>x</sub> radical regeneration in isoprene oxidation via peroxy radical isomerisations. II: experimental  
727 evidence and global impact, *Physical Chemistry Chemical Physics*, 12, 14227-14235, 10.1039/c0cp00811g, 2010.

728 Peeters, J., Muller, J.-F., Stavrou, T., and Vinh Son, N.: Hydroxyl Radical Recycling in Isoprene Oxidation Driven by  
729 Hydrogen Bonding and Hydrogen Tunneling: The Upgraded LIM1 Mechanism, *Journal of Physical Chemistry A*, 118, 8625-  
730 8643, 10.1021/jp5033146, 2014.

731 Ren, X., Olson, J. R., Crawford, J. H., Brune, W. H., Mao, J., Long, R. B., Chen, Z., Chen, G., Avery, M. A., Sachse, G. W.,  
732 Barrick, J. D., Diskin, G. S., Huey, L. G., Fried, A., Cohen, R. C., Heikes, B., Wennberg, P. O., Singh, H. B., Blake, D. R., and  
733 Shetter, R. E.: HO<sub>x</sub> chemistry during INTEX-A 2004: Observation, model calculation, and comparison with previous studies,  
734 *Journal of Geophysical Research-Atmospheres*, 113, 10.1029/2007jd009166, 2008.

735 Shu, L., Wang, T. J., Han, H., Xie, M., Chen, P. L., Li, M. M., and Wu, H.: Summertime ozone pollution in the Yangtze River  
736 Delta of eastern China during 2013-2017: Synoptic impacts and source apportionment, *Environmental Pollution*, 257,  
737 10.1016/j.envpol.2019.113631, 2020.

738 Song, H., Zou, Q., and Lu, K.: Parameterization and Application of Hydroperoxyl Radicals (HO<sub>2</sub>) Heterogeneous Uptake  
739 Coefficient, *Progress in Chemistry*, 33, 1161-1173, 10.7536/pc200749, 2021.

740 Song, H., Lu, K., Dong, H., Tan, Z., Chen, S., Zeng, L., and Zhang, Y.: Reduced Aerosol Uptake of Hydroperoxyl Radical May  
741 Increase the Sensitivity of Ozone Production to Volatile Organic Compounds, *Environmental Science & Technology Letters*,  
742 9, 22-29, 10.1021/acs.estlett.1c00893, 2022.

743 Stevens, P. S., Mather, J. H., Brune, W. H., Eisele, F., Tanner, D., Jefferson, A., Cantrell, C., Shetter, R., Sewall, S., Fried, A.,

744 Henry, B., Williams, E., Baumann, K., Goldan, P., and Kuster, W.: HO<sub>2</sub>/OH and RO(2)/HO<sub>2</sub> ratios during the Tropospheric  
745 OH Photochemistry Experiment: Measurement and theory, *Journal of Geophysical Research-Atmospheres*, 102, 6379-6391,  
746 10.1029/96jd01704, 1997.

747 Stone, D., Whalley, L. K., and Heard, D. E.: Tropospheric OH and HO<sub>2</sub> radicals: field measurements and model comparisons,  
748 *Chemical Society Reviews*, 41, 6348-6404, 10.1039/c2cs35140d, 2012.

749 Stone, D., Evans, M. J., Walker, H., Ingham, T., Vaughan, S., Ouyang, B., Kennedy, O. J., McLeod, M. W., Jones, R. L.,  
750 Hopkins, J., Punjabi, S., Lidster, R., Hamilton, J. F., Lee, J. D., Lewis, A. C., Carpenter, L. J., Forster, G., Oram, D. E., Reeves,  
751 C. E., Bauguitte, S., Morgan, W., Coe, H., Aruffo, E., Dari-Salisburgo, C., Giammaria, F., Di Carlo, P., and Heard, D. E.:  
752 Radical chemistry at night: comparisons between observed and modelled HO<sub>x</sub>, NO<sub>3</sub> and N<sub>2</sub>O<sub>5</sub> during the RONOCO project,  
753 *Atmospheric Chemistry and Physics*, 14, 1299-1321, 10.5194/acp-14-1299-2014, 2014.

754 Taketani, F., Kanaya, Y., Pochanart, P., Liu, Y., Li, J., Okuzawa, K., Kawamura, K., Wang, Z., and Akimoto, H.: Measurement  
755 of overall uptake coefficients for HO<sub>2</sub> radicals by aerosol particles sampled from ambient air at Mts. Tai and Mang (China),  
756 *Atmospheric Chemistry and Physics*, 12, 11907-11916, 10.5194/acp-12-11907-2012, 2012.

757 Tan, Z., Fuchs, H., Lu, K., Hofzumahaus, A., Bohn, B., Broch, S., Dong, H., Gomm, S., Haeseler, R., He, L., Holland, F., Li,  
758 X., Liu, Y., Lu, S., Rohrer, F., Shao, M., Wang, B., Wang, M., Wu, Y., Zeng, L., Zhang, Y., Wahner, A., and Zhang, Y.: Radical  
759 chemistry at a rural site (Wangdu) in the North China Plain: observation and model calculations of OH, HO<sub>2</sub> and RO<sub>2</sub> radicals,  
760 *Atmospheric Chemistry and Physics*, 17, 663-690, 10.5194/acp-17-663-2017, 2017.

761 Tan, Z., Rohrer, F., Lu, K., Ma, X., Bohn, B., Broch, S., Dong, H., Fuchs, H., Gkatzelis, G. I., Hofzumahaus, A., Holland, F.,  
762 Li, X., Liu, Y., Liu, Y., Novelli, A., Shao, M., Wang, H., Wu, Y., Zeng, L., Hu, M., Kiendler-Scharr, A., Wahner, A., and Zhang,  
763 Y.: Wintertime photochemistry in Beijing: observations of RO<sub>x</sub> radical concentrations in the North China Plain during the  
764 BEST-ONE campaign, *Atmospheric Chemistry and Physics*, 18, 12391-12411, 10.5194/acp-18-12391-2018, 2018.

765 Tan, Z., Lu, K., Hofzumahaus, A., Fuchs, H., Bohn, B., Holland, F., Liu, Y., Rohrer, F., Shao, M., Sun, K., Wu, Y., Zeng, L.,  
766 Zhang, Y., Zou, Q., Kiendler-Scharr, A., Wahner, A., and Zhang, Y.: Experimental budgets of OH, HO<sub>2</sub>, and RO<sub>2</sub> radicals and  
767 implications for ozone formation in the Pearl River Delta in China 2014, *Atmospheric Chemistry and Physics*, 19, 7129-7150,  
768 10.5194/acp-19-7129-2019, 2019.

769 Tan, Z., Hofzumahaus, A., Lu, K., Brown, S. S., Holland, F., Huey, L. G., Kiendler-Scharr, A., Li, X., Liu, X., Ma, N., Min,  
770 K.-E., Rohrer, F., Shao, M., Wahner, A., Wang, Y., Wiedensohler, A., Wu, Y., Wu, Z., Zeng, L., Zhang, Y., and Fuchs, H.: No  
771 Evidence for a Significant Impact of Heterogeneous Chemistry on Radical Concentrations in the North China Plain in Summer  
772 2014, *Environmental Science & Technology*, 54, 5973-5979, 10.1021/acs.est.0c00525, 2020.

773 Tan, Z., Ma, X., Lu, K., Jiang, M., Zou, Q., Wang, H., Zeng, L., and Zhang, Y.: Direct evidence of local photochemical  
774 production driven ozone episode in Beijing: A case study, *Science of the Total Environment*, 800,  
775 10.1016/j.scitotenv.2021.148868, 2021.

776 Wang, T., Xue, L. K., Brimblecombe, P., Lam, Y. F., Li, L., and Zhang, L.: Ozone pollution in China: A review of concentrations,  
777 meteorological influences, chemical precursors, and effects, *Science of the Total Environment*, 575, 1582-1596,  
778 10.1016/j.scitotenv.2016.10.081, 2017a.

779 Wang, W., Parrish, D. D., Li, X., Shao, M., Liu, Y., Mo, Z., Lu, S., Hu, M., Fang, X., Wu, Y., Zeng, L., and Zhang, Y.: Exploring  
780 the drivers of the increased ozone production in Beijing in summertime during 2005-2016, *Atmospheric Chemistry and Physics*,  
781 20, 15617-15633, 10.5194/acp-20-15617-2020, 2020.

782 Wang, X., Wang, H., Xue, L., Wang, T., Wang, L., Gu, R., Wang, W., Tham, Y. J., Wang, Z., Yang, L., Chen, J., and Wang, W.:  
783 Observations of N<sub>2</sub>O<sub>5</sub> and ClNO<sub>2</sub> at a polluted urban surface site in North China: High N<sub>2</sub>O<sub>5</sub> uptake coefficients and low  
784 ClNO<sub>2</sub> product yields, *Atmospheric Environment*, 156, 125-134, 10.1016/j.atmosenv.2017.02.035, 2017b.

785 Whalley, L. K., Edwards, P. M., Furneaux, K. L., Goddard, A., Ingham, T., Evans, M. J., Stone, D., Hopkins, J. R., Jones, C.  
786 E., Karunaharan, A., Lee, J. D., Lewis, A. C., Monks, P. S., Moller, S. J., and Heard, D. E.: Quantifying the magnitude of a  
787 missing hydroxyl radical source in a tropical rainforest, *Atmospheric Chemistry and Physics*, 11, 7223-7233, 10.5194/acp-11-  
788 7223-2011, 2011.

789 Whalley, L. K., Stone, D., George, I. J., Mertes, S., van Pinxteren, D., Tilgner, A., Herrmann, H., Evans, M. J., and Heard, D.  
790 E.: The influence of clouds on radical concentrations: observations and modelling studies of HO<sub>x</sub> during the Hill Cap Cloud

791 Thuringia (HCCT) campaign in 2010, *Atmospheric Chemistry and Physics*, 15, 3289-3301, 10.5194/acp-15-3289-2015, 2015.  
792 Whalley, L. K., Slater, E. J., Woodward-Massey, R., Ye, C., Lee, J. D., Squires, F., Hopkins, J. R., Dunmore, R. E., Shaw, M.,  
793 Hamilton, J. F., Lewis, A. C., Mehra, A., Worrall, S. D., Bacak, A., Bannan, T. J., Coe, H., Percival, C. J., Ouyang, B., Jones,  
794 R. L., Crilley, L. R., Kramer, L. J., Bloss, W. J., Vu, T., Kotthaus, S., Grimmond, S., Sun, Y., Xu, W., Yue, S., Ren, L., Acton,  
795 W. J. F., Hewitt, C. N., Wang, X., Fu, P., and Heard, D. E.: Evaluating the sensitivity of radical chemistry and ozone formation  
796 to ambient VOCs and NO<sub>x</sub> in Beijing, *Atmospheric Chemistry and Physics*, 21, 2125-2147, 10.5194/acp-21-2125-2021, 2021.  
797 Xue, L., Gu, R., Wang, T., Wang, X., Saunders, S., Blake, D., Louie, P. K. K., Luk, C. W. Y., Simpson, I., Xu, Z., Wang, Z.,  
798 Gao, Y., Lee, S., Mellouki, A., and Wang, W.: Oxidative capacity and radical chemistry in the polluted atmosphere of Hong  
799 Kong and Pearl River Delta region: analysis of a severe photochemical smog episode, *Atmospheric Chemistry and Physics*,  
800 16, 9891-9903, 10.5194/acp-16-9891-2016, 2016.  
801 Yang, X., Wang, H., Tan, Z., Lu, K., and Zhang, Y.: Observations of OH Radical Reactivity in Field Studies, *Acta Chimica*  
802 *Sinica*, 77, 613-624, 10.6023/a19030094, 2019.  
803 Yang, X., Lu, K., Ma, X., Liu, Y., Wang, H., Hu, R., Li, X., Lou, S., Chen, S., Dong, H., Wang, F., Wang, Y., Zhang, G., Li, S.,  
804 Yang, S., Yang, Y., Kuang, C., Tan, Z., Chen, X., Qiu, P., Zeng, L., Xie, P., and Zhang, Y.: Observations and modeling of OH  
805 and HO<sub>2</sub> radicals in Chengdu, China in summer 2019, *The Science of the total environment*, 772, 144829-144829,  
806 10.1016/j.scitotenv.2020.144829, 2021.  
807 Yang, Y., Wang, Y., Yao, D., Zhao, S., Yang, S., Ji, D., Sun, J., Wang, Y., Liu, Z., Hu, B., Zhang, R., and Wang, Y.: Significant  
808 decreases in the volatile organic compound concentration, atmospheric oxidation capacity and photochemical reactivity during  
809 the National Day holiday over a suburban site in the North China Plain, *Environmental Pollution*, 263,  
810 10.1016/j.envpol.2020.114657, 2020a.  
811 Yang, Y., Wang, Y., Yao, D., Zhao, S., Yang, S., Ji, D., Sun, J., Wang, Y., Liu, Z., Hu, B., Zhang, R., and Wang, Y.: Significant  
812 decreases in the volatile organic compound concentration, atmospheric oxidation capacity and photochemical reactivity during  
813 the National Day holiday over a suburban site in the North China Plain, *Environmental Pollution*, 263, 114657,  
814 <https://doi.org/10.1016/j.envpol.2020.114657>, 2020b.  
815 Yu, D., Tan, Z., Lu, K., Ma, X., Li, X., Chen, S., Zhu, B., Lin, L., Li, Y., Qiu, P., Yang, X., Liu, Y., Wang, H., He, L., Huang,  
816 X., and Zhang, Y.: An explicit study of local ozone budget and NO<sub>x</sub>-VOCs sensitivity in Shenzhen China, *Atmospheric*  
817 *Environment*, 224, 117304, <https://doi.org/10.1016/j.atmosenv.2020.117304>, 2020.  
818 Zhang, Y. H., Hu, M., Zhong, L. J., Wiedensohler, A., Liu, S. C., Andreae, M. O., Wang, W., and Fan, S. J.: Regional Integrated  
819 Experiments on Air Quality over Pearl River Delta 2004 (PRIDE-PRD2004): Overview, *Atmospheric Environment*, 42, 6157-  
820 6173, 10.1016/j.atmosenv.2008.03.025, 2008.  
821 Zhou, J., Murano, K., Kohno, N., Sakamoto, Y., and Kajii, Y.: Real-time quantification of the total HO<sub>2</sub> reactivity of ambient  
822 air and HO<sub>2</sub> uptake kinetics onto ambient aerosols in Kyoto (Japan), *Atmospheric Environment*, 223,  
823 10.1016/j.atmosenv.2020.117189, 2020.  
824 Zhou, J., Sato, K., Bai, Y., Fukusaki, Y., Kousa, Y., Ramasamy, S., Takami, A., Yoshino, A., Nakayama, T., Sadanaga, Y.,  
825 Nakashima, Y., Li, J., Murano, K., Kohno, N., Sakamoto, Y., and Kajii, Y.: Kinetics and impacting factors of HO<sub>2</sub> uptake onto  
826 submicron atmospheric aerosols during the 2019 Air QUALity Study (AQUAS) in Yokohama, Japan, *Atmospheric Chemistry*  
827 *and Physics*, 21, 12243-12260, 10.5194/acp-21-12243-2021, 2021.  
828 Zhu, J., Wang, S., Wang, H., Jing, S., Lou, S., Saiz-Lopez, A., and Zhou, B.: Observationally constrained modeling of  
829 atmospheric oxidation capacity and photochemical reactivity in Shanghai, China, *Atmospheric Chemistry and Physics*, 20,  
830 1217-1232, 10.5194/acp-20-1217-2020, 2020.

带格式的: 字体: (默认) Times New Roman

带格式的: 字体: (默认) Times New Roman

带格式的: 字体: (默认) Times New Roman

带格式的: 字体: (默认) Times New Roman

域代码已更改

831